Facultade de Ciencias do Mar
Universidade de Vigo

ESTUDIO DE FACTORES BIÓTICOS Y ABIÓTICOS EN LOS DESPRENDIMIENTOS DE MEJILLÓN EN BATEAS (RÍA DE AROUSA)/ STUDY OF BIOTIC AND ABIOTIC FACTORS IN MUSSEL DISLODGEMENTS IN AQUACULTURE RAFTS (RÍA DE AROUSA)

EVETTE LOREAL PEREZ

Curso Académico 2022/2023
Convocatoria de: Julio

Tutores: José M. Fernández Babarro, Miguel Gil Coto

TABLE OF CONTENTS

LIST OF TABLES AND FIGURES

ABSTRACT

Distinct environmental conditions across the Ría de Arousa result in abiotic gradients and unique responses in raft-cultivated blue mussel *Mytilus galloprovincialis* assemblages. Dislodgement of *M. galloprovincialis* may occur for a variety of reasons including predation and wave-action generated lift or drag, resulting in economic losses. In addition, previous studies have documented the detrimental effects of biofouling by the sea anemone *Actinothoe sphyrodeta* on the protective tissues of *M. galloprovincialis* in this region. This study characterizes sitewide trends in abiotic and biotic factors influencing the dislodgement of raft-cultivated *M. galloprovincialis* over three consecutive cultivation cycles in the Ría de Arousa. To explore differential responses in *M. galloprovincialis* mediated by the environment, several mussel response parameters were analyzed using inferential statistical methods. Sites with greater hydrodynamic conditions experienced substantial mussel dislodgements or biomass losses when extensively colonized by the epibiont *A. sphyrodeta*. Multiple regression analysis indicated biofouling by this anemone was the most significant ($p < 0.001$) factor in predicting mussel protective tissue (byssus tenacity and shell thickness index) models, while food availability was the most significant ($p < 0.001$) in a soft tissue status (condition index) model. Soft tissues displayed great variability throughout the study period and ANCOVA analysis revealed only significant differences ($p < 0.01$) with shell length, indicating that endogenous processes (i.e., sexual maturation, spawning, etc.) exert a stronger influence than environmental drivers in this mussel response. Mussel responses exhibited environment-mediated energetic tradeoffs throughout the study period, but further studies are needed to continue long-term surveillance of biofouling incidence and its synergistic effects with environmental parameters in predicting future raft-cultivated mussels biomass losses or dislodgements in this region.

Keywords: *Mytilus galloprovincialis*, byssus, tenacity, condition index, shell thickness index, energetic tradeoffs, time lags, biofouling

RESUMEN

Las diferentes condiciones ambientales a lo largo de la Ría de Arousa generan gradientes de factores abióticos y respuestas únicas en los mejillones azules *Mytilus galloprovincialis* cultivados en bateas. Los desprendimientos de *M. galloprovincialis* pueden ocurrir por una variedad de razones, incluyendo la depredación y el movimiento o el arrastre provocados por la acción de las olas, lo que genera pérdidas económicas. Además, estudios previos han documentado los efectos perjudiciales que la anémona de mar *Actinothoe sphyrodeta* produce en los tejidos protectores de *M. galloprovincialis* en esta región. Este estudio caracteriza las tendencias en varios puntos de muestreo de los factores abióticos y bióticos que influyen en los desprendimientos de *M. galloprovincialis* cultivado en batea durante tres ciclos de cultivo consecutivos en la Ría de Arousa. Para explorar las distintas respuestas al entorno que da *M. galloprovincialis*, se utilizaron métodos de inferencia estadística en varios de sus parámetros de respuesta. Cuando hay proliferaciones del epibionte *A. sphyrodeta* las bateas expuestas a

condiciones hidrodinámicas más energéticas registran más desprendimientos y pérdida de biomasa de mejillón. El análisis de regresión múltiple aplicado indicó que la biofouling de esta anémona fue el factor más significativo ($p < 0,001$) en la predicción de modelos de tejido protector de mejillón (tenacidad de biso y índice de espesor de concha), mientras que la disponibilidad de alimento fue el más significativo ($p < 0,001$) en un modelo de estado de tejido blando (índice de condición). Los tejidos blandos mostraron una gran variabilidad a lo largo del período de estudio y el análisis ANCOVA reveló solo diferencias significativas ($p < 0,01$) con la longitud de la concha, lo que indica que los procesos endógenos (i.e., maduración sexual, desove, etc.) ejercen una influencia más fuerte que los factores ambientales en esta respuesta del mejillón. Las respuestas de los mejillones exhibieron balances energéticos mediados por el medio ambiente durante todo el período de estudio, pero se necesitan más estudios para continuar con la vigilancia a largo plazo de la incidencia de biofouling y sus efectos sinérgicos con los parámetros ambientales para predecir futuras pérdidas de biomasa o desprendimientos de mejillones en los cultivos en batea de esta región.

Palabras clave: *Mytilus galloprovincialis,* biso, tenacidad, índice de condición, índice de espesor de concha, balances energéticos, lapsos de tiempo, biofouling

1. INTRODUCTION

The Rías Baixas in Galicia, Spain are four highly productive embayments located along the northwestern Iberian Peninsula that formed as a result of a series of tectonic movements and climatic processes during the Alpine uplift (González-Garcés Santiso et al., 2008). The Galician coast defines the northern perimeter of the North Atlantic Eastern Boundary Upwelling System (Arístegui et al., 2009), an area characterized by seasonal oscillations between the upwelling of nutrient-rich Eastern North Atlantic Central Water and the downwelling of superficial waters (Alvarez-Salgado et al., 2000; Rosón et al., 1995; Rosón et al., 1997). Coastal upwelling, through offshore Ekman transport, is driven at these latitudes by the predominance of northerly winds from approximately March to October generating ideal productive conditions for aquaculture (Blanton et al., 1987; Fraga, 1981; Figueiras et al., 2002).

Modern mussel cultivation techniques in the Rías Baixas evolved in the 20th century (Mexillón de Galicia, 2023b) to yield peak annual production rates during the late 1990s before dwindling to current levels of >200,000 tonnes (FAO, 2023). Over 90% of the total Spanish mussel production is cultivated in Galicia, leading annual production rates in Europe and worldwide (FAO, 2022). The mussel species cultivated in Galicia is *Mytilus galloprovincialis* (Lamarck, 1819), an indigenous marine bivalve mollusc from the family Mytilidae commonly known as the Mediterranean mussel (MolluscaBase eds, 2023). *Mytilus galloprovincialis* are filter feeders that graze on phytoplankton, prefer rocky substrates, and serve as a foundation species in littoral ecosystems (Suchanek, 1992). Suspension-cultivated *Mytilus*

galloprovincialis in the Rías Baixas are subject to varying abiotic and biological conditions that may influence their success in a highly heterogeneous coastal environment (Carrington, 2002; Zardi et al., 2007; Lachance et al., 2008; Babarro and Reiriz, 2010; Babarro and Lassudrie, 2011; Babarro and Carrington, 2013; Babarro et al., 2019).

While capable of small micromovements on a wide variety of substrates, *Mytilus galloprovincialis* are largely sessile organisms that live in clusters or aggregations attached to hard substrates and each other by a filamentous collagen-type proteinaceous tissue called byssus. Secreted by the foot organ (Waite, 1992), byssus is capable of attaching to virtually any substratum through adhesive plaques located at its distal section while the proximal tissue connects to a common stem (Floriolli et al. 2001). Byssal attachment is imperative for the mussel to avoid dislodgement by predation or wave action-generated lift or drag (*Figure 1*) (Bell and Gosline, 1997; Denny, 1987), which would result in certain mortality, and to the succession of mussel beds by outcompeting other species for space or food through the formation of large assemblages (Denny, 1987; Babarro and Abad, 2013). Byssus secretion and strength displays seasonal variation (Lachance et al., 2008; Carrington et al., 2009) as well as plastic properties in both mechanical and compositional features such as extensibility, modulus, mechanical stress, yield, and amino acid composition (Babarro and Reiriz, 2010; Babarro and Carrington, 2011; Babarro and Carrington, 2013). Mussels respond to changing environmental conditions by increasing byssus attachment strength through thread reinforcement or enacting structural changes to secure better attachment (Floriolli et al., 2001; Babarro and Carrington, 2011). For example, mussels cultivated in the intertidal environments of the Rías Baixas have been observed to increase the secretion of thicker and stronger byssus in response to greater hydrodynamic forces (Babarro and Carrington, 2013). Byssus production may entail up to 15% of a mussel's average energetic expenditure (Griffiths and King, 1979; Hawkins and Bayne, 1985). While mussels secrete individual byssus threads in only minutes, their quality typically decays over time and are replaced after some 8 weeks, though this time span decreases to a fraction of that during warmer temperatures in the summer (Bell and Gosline, 1996; Moeser and Carrington, 2006).

Studies examining mussel attachment strength often normalize these values against mussel size obtaining a parameter known as tenacity. Due to the growth effect, mussel tenacity exhibits a slope inverse to that of attachment strength (citations). While attachment strength, or force, increases with mussel size, tenacity decreases because the shell growth (area) occurs at a greater rate than that of attachment force (Bell and Gosline, 1996, 1997; Qin and Buehler, 2013). Mussel tenacity is mediated by hydrodynamic stress (Babarro and Carrington, 2011; Babarro and Lassudrie, 2011; Babarro and Carrington, 2013; Babarro et al., 2020). Juvenile mussels are capable of strong attachment in part due to their overall small shell area but also because of their sexual immaturity, precluding them from high energetic reproduction demands, which can reach up to 90% of total expenditures and result in detrimental mussel performance (Carrington, 2002). Attachment strength can also be impacted by biofouling, the accumulation of small

organisms, or epibionts, on surface areas (Garner and Litvaitis, 2016). Biofouling mechanisms include epibiont competition for mussel food (Lesser et al., 1992; Sievers et al., 2013) or inhibition of byssus production (Garner and Litvaitis, 2016). In the Ría de Arousa, epibiosis of the marine anemone *Actinothoe sphyrodeta* was correlated with diminished byssus tenacity in raft-cultivated mussels, inducing poor performance that resulted in dislodgements (Babarro et al., 2019).

Another critical component to mussel survival is its hard calcium carbonate shell. The shell encompasses the mussel soft tissues, providing protection from predators, destructive hydrodynamic forces, and the elements during low tide in intertidal zones (Raubenheimer and Cook, 1990; Akester and Martel, 2000; Steffani and Branch, 2003; Beadman et al., 2003). Shells also provide valuable information as an indicator of mussel growth, with several studies reporting environment-mediated shell growth and morphology parameters (Raubenheimer and Cook 1990; Akester and Martel 2000; Steffani and Branch 2003; Beadman et al. 2003; Babarro and Carrington, 2011; Babarro and Carrington, 2013). The shell thickness index (STI) integrates shell morphology parameters including the anteroposterior (shell length), dorsoventral (shell height) and lateral axes (shell width) (*Figure 2*) and the shell weight (Freeman et al., 2009). Since shell tissue is crucial to mussel survival and may require up to 50% of a mussel's total energy expenditures to thicken and grow (Gardner and Thomas, 1987), the STI is often studied in conjunction with other growth indicators in environment-modulated energy allocation routes.

A common indicator of mussel nutritional status and gonadal state is the condition index, an estimation for the total soft tissue amount. Blanton et al. (1987) first correlated mussel condition index with upwelling in the Rías Baixas, specifically the Ría de Arousa, highlighting the interannual variability and the potential use of synoptic scale weather patterns in predicting mussel production. Mussel soft tissues may entail up to 50% of energetic expenditures (Fuentes-Santos et al., 2019). Larger mussels are inclined to greater condition index values though tradeoffs between soft tissue growth and protective tissue growth (i.e., shell and byssus) occur in hydrodynamically exposed environments (Babarro and Carrington, 2011). Condition index, reflecting the amount of soft tissue per unit of shell, is commonly used in market valuations of cultivated bivalves (Watanabe and Katayama, 2010; Martinez et al., 2018) and is greatly influenced by mussel endogenous rhythms linked to sexual maturity, spawning processes, and gonad restoration actions (Babarro and Carrington, 2011).

As upwelling bays (Largier, 2020), the semi-enclosed environments in the Rías Baixas are influenced by synoptic scale upwelling winds, local winds, midlatitude climatology modes in the North Atlantic, and estuarine circulation driven by continental runoff and temperature exchange with the atmosphere (Blanton et al., 1984; Fraga, 1981; Alvarez-Salgado et al., 2000; Pérez et al., 2010; Pardo et al., 2011). Superficial waves in the Rías Baixas are driven by wind regimes governed by two climatology modes (Villacieros-Robineau et al., 2021): the West Europe Pressure Anomaly (WEPA), a climate index associated with coastal Atlantic winter wave height, is based on differences in sea level pressure between atmospheric stations located

in the Canary Islands and Ireland (Castelle et al., 2017), and the North Atlantic Oscillation (NAO), a climate index associated with representing the difference in atmospheric sea level pressure between the Azores High and the Icelandic Low systems (Barnston and Livezey, 1987).

The purpose of this work is to characterize sitewide trends in raft-cultivated *Mytilus galloprovincialis* over three consecutive cultivation cycles in the Ría de Arousa. The objectives include describing the temporal and spatial variability of key biotic and abiotic factors in the Rías Baixas and their impact on mussel biological responses along growth cycles. Integrating mussel responses (e.g., marketable value and protective tissues) would provide insight into sitewide vulnerability to cultivation rope dislodgements or natural predation resulting from weaker byssus strength or shell tissues. Moreover, such integrations would identify potential site-specific tradeoff dynamics impacting mussel fitness, growth, and survival. Site-specific heterogeneity within the ría may induce ecological conditions that may represent crucial drivers of mussel performance in an intensely cultivated area (Ría de Arousa, NW Iberian Peninsula). Obtained results are discussed within the framework of understanding the principal environmental drivers that modulate raft-cultivated mussel biological responses with the intent to minimize cultivated biomass losses or promote scientific knowledge that leads to better practices.

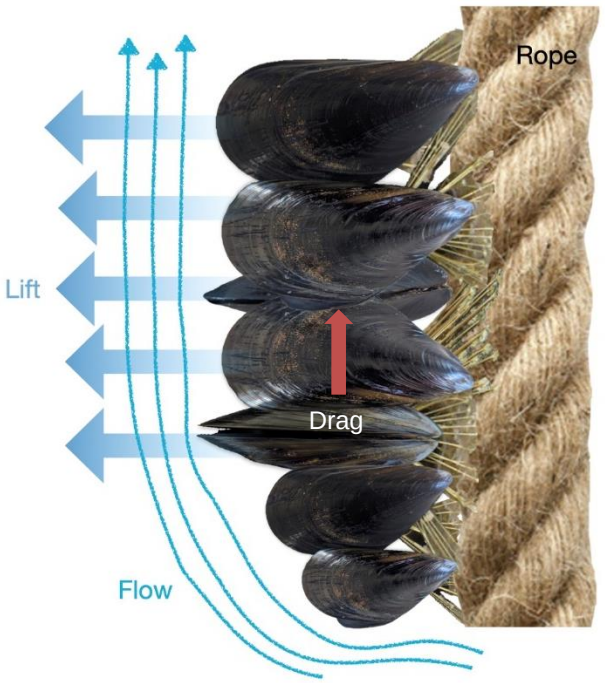

Figure 1. Schema of lift and drag forces exerted on mussel beds by water currents. Adapted from Denny and Gaylord, 2010, copyright 2010 by Annual Reviews.

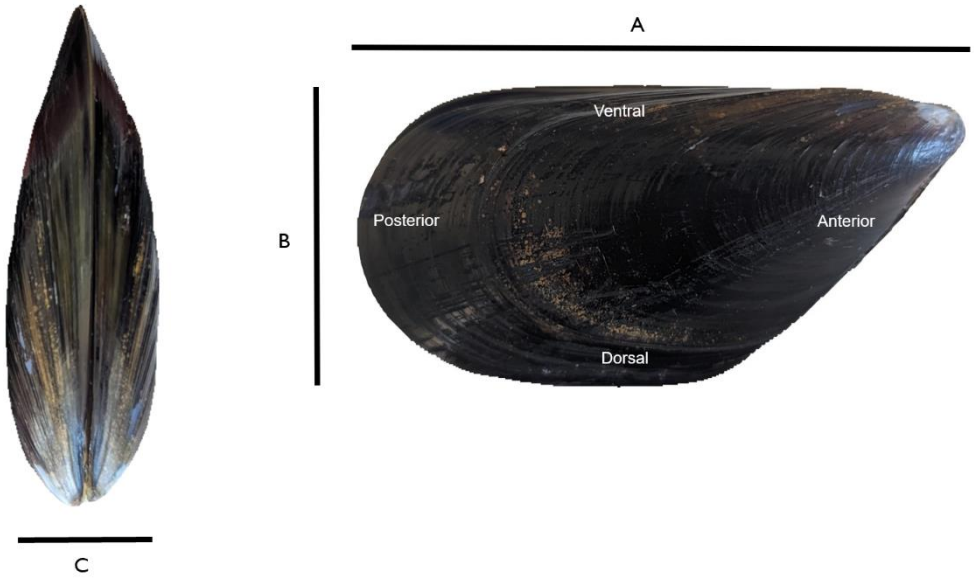

Figure 2. Shell morphology of Mytilus galloprovincialis displaying the A) anteroposterior (shell length), B) dorsoventral (shell height) and C) lateral axes (shell width).

2. MATERIALS AND METHODS

2.1. Study site

The Ría de Arousa is the largest of the Rías Baixas with a total volume of 4300 m3 extending 25 km in longitude from Sálvora Island to the mouth of the estuary of the Río Ulla, while reaching maximum depths of 70 m (Otto, 1975). It comprises a surface area of 230 km2 containing more than 2300 mussel cultivation rafts, representing ~69% of the total rafts located throughout Galicia (Mexillón de Galicia, 2023a).

Despite being an estuary with a mesotidal regime, tidal range of 1.5 and 3.7 m (Otto, 1975; Rosón et al., 1995), the key forcing of the Ría de Arousa is the coastal upwelling and its modulation by the ría bathymetry (Rosón et al., 1997). Just as occurs across all four Rías Baixas (Álvarez-Salgado et al., 2000), the Ría de Arousa operates as an extension of the shelf during upwelling events with both wind and river driven circulations reinforcing each other and setting a positive bidirectional two-layer flow (surface freshwater leaving the ría and bottom saltier water entering the ría) along the ría. In downwelling events, the wind circulation opposes the river-induced circulation and the external part of the ría exhibits a negative circulation wherein surface water enters the ría while bottom water leaves the ría; simultaneously, the internal ría maintains a river-induced positive circulation. Upwelling winds are more frequent from March/April to September/October, the upwelling season, whereas downwelling winds prevail the remainder of the year, the downwelling season. However, it’s not rare to observe upwelling

and downwelling events during both seasons (Blanton et al., 1987).

The Ría of Arousa's central axis lies along a southwest-northeast orientation permitting the entrance of western and southwestern waves, as demonstrated by studies in nearby Ría de Vigo (Villacieros-Robineau et al., 2021), with Sálvora Island forming a barrier at the mouth as the Cíes Islands do in the Ría de Vigo. Given the wave field behavior in the Ría de Vigo, it's theorized that as swell propagates into the Ría de Arousa from the continental shelf, its height will be similarly attenuated by the coastal geomorphology while in situ ría-generated wind sea waves dominate the total wave height inside the ría (Otto, 1975). Winter wave height maxima characterized by negative NAO and positive WEPA index values are also anticipated as these two climate modes also account for over 90% of the variability in mean wave parameters in the nearby Ría de Vigo (Villacieros-Robineau et al., 2021).

The ría hydrography was described using thermohaline data gathered across eleven sites sampled by the Instituto Tecnolóxico para o Control do Medio Marino (INTECMAR) at www.intecmar.gal. The surface water temperatures range between maxima approaching 22 °C in the interior and minima reaching 10 °C. Salinity maximum values reach 36.5 psu in surface waters during events of maximum evaporation while continental runoff from the Umia and Ulla rivers and rainfall drive minimum salinities of less than 10 psu in the ría interior. Annual total river discharge values average 61 m3·s-1 but can reach as high as 140 m3·s-1 during the rainy winter season (Otto, 1975). However, the upwelling season and individual upwelling events fertilize the ría with the influx of nutrients that fuel phytoplankton growth, resulting in average gross primary production values of ~1.4 g of $C \cdot m^{-2} \cdot d^{-1}$, though values as high as 4 g of $C \cdot m^{-2} \cdot d^{-1}$ can be observed on shorter temporal scales when the limitation of phytoplankton advection to the shelf results from upwelling relaxation events (Figueras et al., 2002).

2.2. Experimental design and sampling

Experimental samples were taken at four geographically representative sites in the Ría of Arousa (*Figure 3*): two located at the mouth of the estuary representing the northern (OuN) and southern (OuS) exterior sites, a central site along the longitudinal axis located about midway from the exterior and interior (MidW), and a site located at the furthermost interior of the ría (InC). Due to exposure to the open sea, the outer sites are subjected to greater hydrodynamic forces and while the interior sites are sheltered from the open ocean, they are subject to estuarine circulation generated from discharge by the Umia and Ulla rivers (Otto, 1975; Rosón et al., 1997).

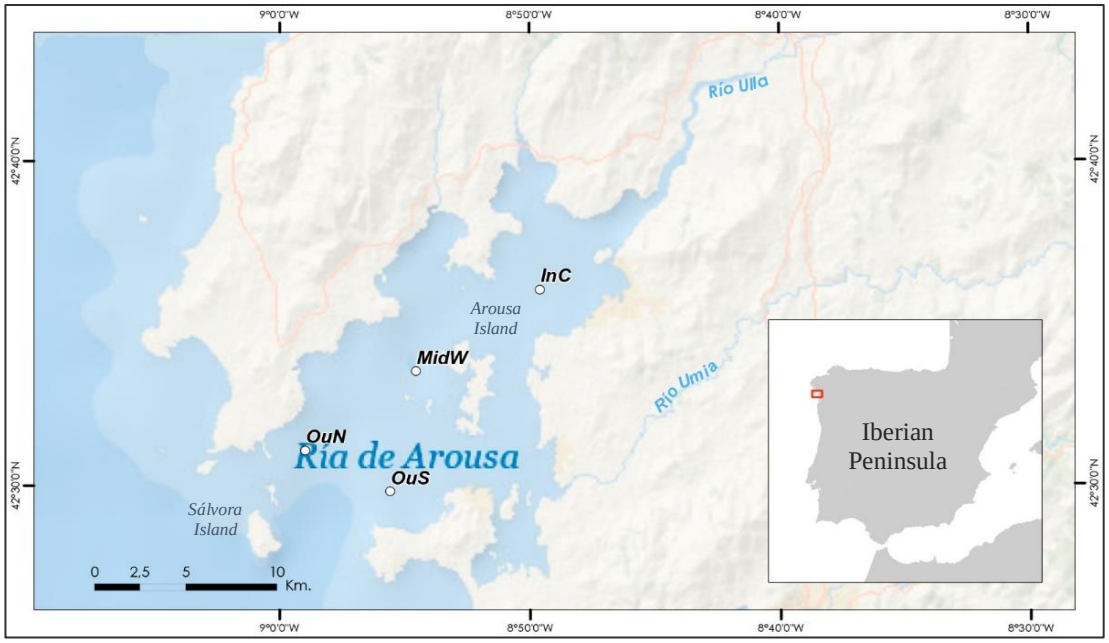

Figure 3. Experimental sites in the Ría of Arousa: outer sites at the northern (OuN) and southern (OuS) mouth, a midcentral site (MidW) to the west of Arousa Island, and the innermost site (InC). Sálvora Island is located at the mouth while the Ulla and Umia rivers flow into the ría from the northeast and southeast, respectively.

Mytilus galloprovincialis were cultivated on experimental ropes fastened to rafts located at four distinct sites in the Ría de Arousa (*Figure 3*). At each site, a raft containing six 12-m long ropes suspended from the aft was designated for monthly sampling. Each raft, measuring 20 x 25 m, is kept afloat by a system of buoyant devices, anchored by an iron chain at its bow and supports up to 500 ropes. All ropes are maintained separate at a distance of 1 m to ensure adequate growth, and initial population densities for each rope averaged 900 mussels per m. The cultivation cycle typically lasts about 18 months consisting of two periods: a seeding to thinning-out process followed by a thinning-out to harvest process. The seeding process is initiated when juvenile mussels, also known as spat, are collected from natural populations within the rías during winter. The spat is affixed to ropes using a covering consisting of a biodegradable adhesive net where they remain for four to six months until they have roughly doubled in size. After reaching 45 to 50 mm, the mussels are removed from their original ropes and deposited onto two or three new ropes in a process known as thinning-out, where a sparser distribution fosters conditions conducive to their growth. The mussels are bound to their new rope by a biodegradable net. The risk of rope dislodgement is greater during the second cultivation stage, a consequence of the greater impact of the hydrodynamic stress and biofouling incidence on older, heavier, and larger mussels that are weakly attached (Babarro et al., 2018). Mussels grow on the ropes until experimentally sampled during this stage upon reaching commercial sizes, typically ≥50 mm.

Three consecutive mussel cultivation cycles were monitored at each of the four experimental sites during the study period. The 1st cycle extended from September 2015 to

August 2016, the 2nd cycle extended from October 2016 to August 2017, and the third cycle extended from December 2017 to October 2018. A monthly sampling was carried out along a single rope each month for all sites at depths of 1, 3, 5, 7, 9 and 11 meters. Ropes were alternated each month ensuring representative samplings of all ropes at each site over the study period. At each sampled depth, individual mussels (n=10) were selected from the outer areas of the mussel assemblages for use in attachment strength and tenacity measurements (see section 2.3. below). An additional cluster of mussels (typically 300-400 mussels, mean n= 387.98±74.99) was sampled along the experimental depths and maintained at the laboratory for use in determining the condition index and shell thickness index (see sec. 2.4. and 2.5. below). High resolution photographs of the ropes were taken in the field to document the presence of epibiontic species (see sec. 2.6. below). Weight measurements for sampled ropes were taken in the field while clusters and individual mussels were weighed in the laboratory (see sec. 2.7. below).

2.3. Tenacity

Individual mussels were selected from the outer regions of the mussel assemblages as their accessible position made it easier to determine the byssus attachment force without disturbing adjacent mussels. Following the method by Denny (1987) for attachment force determination, a spring scale (Digital Force Gauge DN431, PCE Iberica S.L. Alicante, Spain, 0.01 N resolution) was attached to individual wet mussels using custom-made forceps as described by Babarro and Comeau (2014) and pulled 90° to the substratum until dislodgement occurred. Mussels adjacent to those selected for dislodgement were disqualified from sampling if found to have byssus threads interconnected between them. The mussels were sampled in the field under wet conditions to prevent the structural modification of the byssus mechanical properties (Babarro et al., 2019). Subsequently, Vernier calipers (accuracy resolution of ±0.1 mm) were used to measure the anteroposterior (shell length), dorsoventral (shell height) and lateral axes (shell width) of the sampled mussels (*Figure 2*).

As a consequence of continuous mussel growth throughout the study period, the byssus tenacity was calculated by normalizing byssus attachment force to individual mussel size using the Bell and Gosline (1997) approximation for shell projected area (A_P). This method estimates the dislodged mussel A_P as an ellipse using the product of shell width and height values. Tenacity (TEN) is measured in $N \cdot m^{-2}$ according to the formula:

$$\text{TEN} = \frac{F}{A_p} \qquad \text{(Equation 1)}$$

where F is the attachment force (N) and A_P is the shell projected area (m^2).

2.4. Condition Index

Mussel condition index (CI) values were obtained according to Freeman et al. (1974) who defined CI as the relationship between the mussel soft tissue weight and its shell weight as follows:

$$CI = \frac{DW_{tissue}}{DW_{shell}} \cdot 100 \quad \text{(Equation 2)}$$

where DW_{tissue} is the dry weight (kg) of the tissues and DW_{shell} is the dry weight (kg) of the shell. To obtain dry weight values, the soft tissue is removed from the shell, and both are dried separately in an oven at 60 °C for 48 h.

2.5. Shell Thickness Index

The shell thickness index (STI) integrates the mussel shell weight and its dimensions (i.e., area) as defined by Freeman et al. (2009):

$$STI = \frac{DW_{shell}}{0.5 \cdot L\,(H^2 + W^2) \cdot \frac{\pi}{2}} \cdot 1000 \quad \text{(Equation 3)}$$

where DW_{shell} is the dry weight (kg) of the shell, L is the shell length (mm), H is the shell height (mm) and W is the shell width (mm).

2.6. Biofouling surveillance

The presence of biofouling, or epibiosis, on cultivation ropes was monitored throughout the study period. Among various species attached to raft-cultivated mussel assemblages, the sea anemone *Actinothoe sphyrodeta* was selected in the present study as a key species for temporal and spatial analysis. Once the sampled rope was lifted onto the boat and weighed, digital photographs were taken of the entire rope at the experimental depth intervals of 1, 3, 5, 7, 9 and 11 m to document the incidence of epibiontic organisms using a Nikkor 18–55 mm lens on a Nikon D3100 camera (Nikon Inc., NY, USA). Clusters of mussels at the experimental depths were randomly sampled for presence of biofouling and scored from 0 to 4 following the schema defined by Babarro et al. (2019) for shell area epibiosis. Camera and light settings were maintained constant throughout the study period.

2.7. Biomass estimation

Mussel biomass was estimated from mussel live weight on cultivated ropes. Mussel live weight was measured by two digital dynamometers (Jaguar™, S.A.L. Villabona, Guipúzcoa, Spain, with an accuracy resolution of 0.1 kg and weight constraints of 100 and/or 1,000 kg) following the method outlined by Babarro et al. (2019) for determining stable weight values with video recording. Mussel live weight on submerged ropes was recorded before raising the rope onto the boat and repeating the measurement by air.

Mussel aggregations along the rope were sampled at the experimental depths (1, 3, 5, 7, 9, and 11 m) and prepared for later analysis at the laboratory. The sampled clusters represented approximately 3–4% of the live weight of the experimental rope. Rope live weight and number of mussels per cluster were noted for each sampling date and site. At the laboratory, epibiontic organisms were removed from the sampled clusters before individual mussel measurements and weight were taken.

Mussel biomass loss is determined as the difference between the theoretical maximum weight and the observed live weight, assuming a constant population density throughout the cultivation cycle. The theoretical maximum weight (mw) assumes no incidence of mortality or dislodgements, is measured in and is calculated as follows:

$$mw = d_{t0} \cdot \frac{W}{n} \cdot \text{m of rope} \qquad \text{(Equation 4)}$$

where d_{t0}=900 is the initial population density of individuals per m of rope, W is the weight (kg) of the sampled cluster, n is the total number of mussels sampled in the cluster, and m of rope=12 is the length of the experimental rope (m).

2.8. Environmental characterization

The numerical model, Regional Ocean Modeling System (ROMS/ CROCO) was configured with a multiple-nested grid constructed using two-way nesting between the domains to simulate interchange between the Ría de Arousa and the ocean. The resolution was increased with an Adaptive Grid Refinement In Fortran (AGRIF) following the method by Debreu et al. (2012). The ROMS model was forced with surface wind, radiation, precipitation, air temperature and humidity variables from the MeteoGalicia interpolation of the Weather Research and Forecasting (WRF) regional model, tidal parameters from the Oregon State University TOPEX/Poseidon Global Inverse Solution (Egbert and Erofeeva, 2002) TPXO global tidal model, and river runoff from the MeteoGalicia configuration of the Soil and Water Assessment Tool (SWAT). The output used in the present study consisted of current velocity, temperature and salinity data averaged over a depth interval of 0-12 m. Output was generated hourly and averaged over 24 hours to obtain daily mean values. Four hindcasts (or lagged-averages time series of daily mean values further averaged into time-windows taken prior to, and including, each original date) of 7, 15, 30 and 45-day intervals were also generated. Temperature and salinity output data were validated against data provided by the Instituto Tecnolóxico para o Control do Medio Mariño de Galicia (INTECMAR) CTD stations located within the Ría of Arousa.

Food availability was approximated by multiplying the chlorophyll a (chl-a) concentration, a proxy for phytoplankton biomass, and the current velocity. Daily chl-a measurements were obtained through satellite observations from the Sea-viewing Wide Field-of-view Sensor (SeaWiFS) Level-3 Standard Mapped Image data provided by the Distributed Active Archive Center at the NASA Goddard Space Flight Center. Current velocity data was obtained from the ROMS/CROCO model output.

The Simulating Waves Nearshore (SWAN) numerical model, from Delft University of Technology (The SWAN Team, 2022), was configured by MeteoGalicia with an unstructured grid to determine wave parameters from its forecast power spectra in the regional domain of the Galician coasts. The SWAN model was forced with the MeteoGalicia WRF in order to propagate the MeteoGalicia Wave Watch III (WW3DG, 2019) large-scale numerical wave

simulations into a higher resolution grid and increase the model performance in the Ría of Arousa. The SWAN numerical model output was utilized to calculate the total wave power (P_w, $W \cdot m^{-1}$) within the ría using the formula:

$$P_w = E \cdot C_g \quad \text{(Equation 5)}$$

where the wave energy, $E = 1/8 \cdot g \cdot \rho_{water} \cdot H_s^2$ in Joules (J), C_g ($m \cdot s^{-1}$) is the celerity of the group of waves that depends on the period and wavelength, g is the gravitational force = 9.8 $m \cdot s^{-2}$, ρ_{water} is the density of water ($kg \cdot m^{-3}$), and H_s is the significant wave height (m). Wave power and wave height data output was generated hourly and averaged over 24 hours to obtain daily mean values. Four hindcasts of 7, 15, 30 and 45-day intervals were also generated.

Monthly means of the well-known (Bakun, 1973; Lavin et al., 1991) upwelling index (UI), data provided by the Indice de Afloramiento database at the Instituto Español de Oceanografía (IEO) was used to characterize the seasonal and annual upwelling and downwelling patterns. Downwelling was recorded as negative UI values ($m^3 \cdot s^{-1} \cdot km^{-1}$). Monthly means were averaged over the upwelling (April to September) and downwelling seasons (January to March and October to December) to obtain annual values.

Monthly mean river discharge data ($m^3 \cdot s^{-1}$) for the Ulla and Umia rivers during the study period was obtained from the network of river gauging stations managed by MeteoGalicia. Following the unavailability of river discharge data for the Umia river for the third cultivation cycle, a simple regression model was generated using the first two years of the study period to extrapolate Umia river discharge values for the third cycle. The linear regression equation was Umia = 2.131· Ulla + 3.5926 with a high, and significant correlation coefficient of $r^2 = 0.9221$.

2.9. Statistical analysis

A univariate analysis of covariance (ANCOVA) was employed to test for significant effects and potential interactive effects of independent factors (i.e., cultivation site and cycle) on mussel biological responses using mussel shell length as a covariable. A Levene test was employed to evaluate data for homogeneity of variance. When required, data was log-transformed before proceeding. If heterogeneity persisted, rank transformation was applied as indicated by Conover (2012). A Tukey's *post hoc* test was performed to determine significant variations between experimental groups. Linear regression models were used to evaluate the relationship between mussel biological response variables and shell length for each experimental site and cultivation cycle. Multiple regression analysis was used to determine the potential significant effects of site-mediated environmental parameters on key mussel biological responses. Since the mussel biological responses studied here vary at different temporal scales (from minutes to months) the environmental parameters were time lagged, averaging specific past periods (lagged averages or hindcasts of 7, 15, 30 and 45-day time windows) when applied in multiple regression models. Mussel raft geographical positions expressed in latitude, and longitude (in negative westward values from the prime meridian), a quantitative representation

of the experimental sites, were used to test potential sitewide effects in multiple regression models. All analyses were performed using STATISTICA 7.0 software (TIBCO Software Inc., Palo Alto, CA, U.S.A.), Excel software (Microsoft Corp., Redmond, WA, U.S.A.), and SPSS Statistics 23 (IBM España S.A., Madrid, Spain).

3. RESULTS

3.1. Environment

3.1.1. Temperature

The temporal variability of temperature averaged across depths from 0 to 12 m, over the three cultivation cycles for all experimental sites is shown in *Figure 4*. Temperature values throughout the study period ranged between 12.24 and 17.88 °C, demonstrating a seasonal periodicity at all experimental sites. The innermost site (InC) experienced the greatest variability registering both the lowest and highest temperatures. The temperature curves display seasonal nadirs just after the onset of boreal spring (MAM) resulting from the upwelling of deep, cold water as confirmed by the time evolution of the UI (*Figure 5*). Interannual variability demonstrates generally more attenuated temperature differences during the boreal winter (DJF)-spring transition in the second and third cultivation cycles, with the least variations observed at the exterior sites (OuN and OuS) during the third cycle which coincides with increasing UI values over the same period (*Figure 4*). Summer (JJA) temperature maximums were observed during the second cultivation cycle at all sites, while winter temperature minimums occurred during the first cultivation cycle for all sites. An outer-to-inner gradient displaying colder temperatures at the interior sites is observed during winter (DJF) of all cultivation cycles that coincides with periods of downwelling (*Figure 4*). During the second cycle, the extension of this winter gradient into early spring coincides with downwelling over the same period (*Figure 5*). An inverse of this geographical pattern, wherein warmer temperatures observed at the interior sites during the summer (JJA) and autumn (SON) months also coincides with periods of upwelling (*Figure 4*).

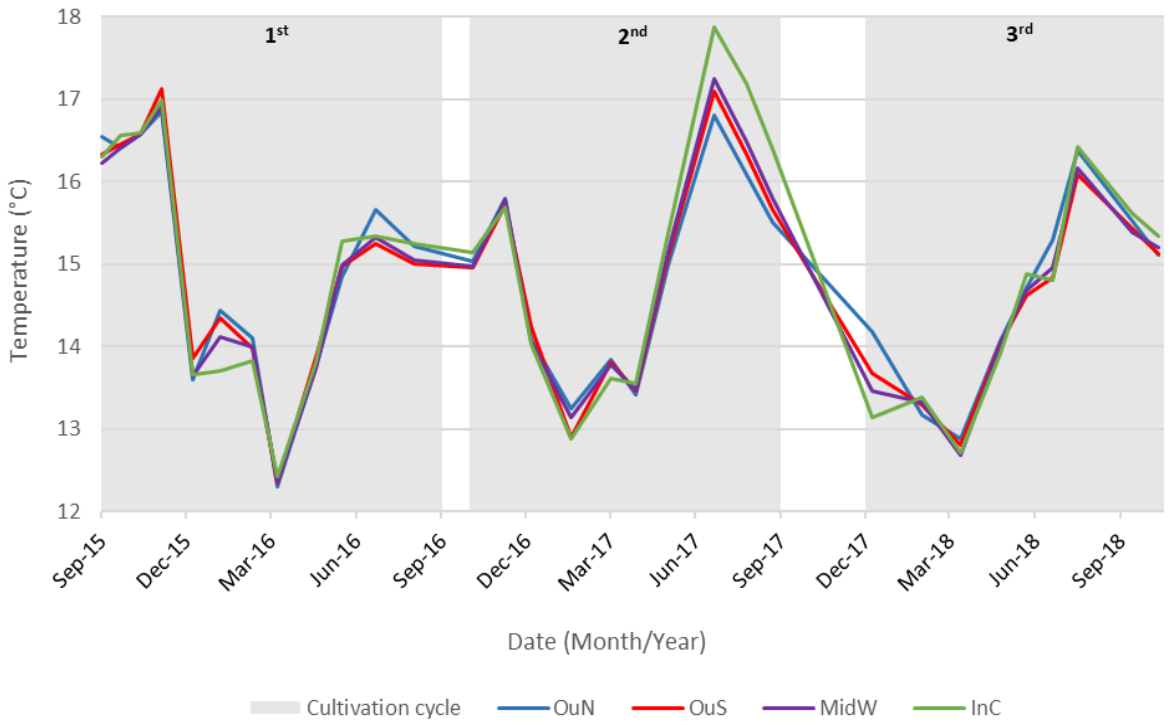

Figure 4. Time series plot containing seven-day hindcasts of mean temperature values (°C) for the four experimental sites over the study period.

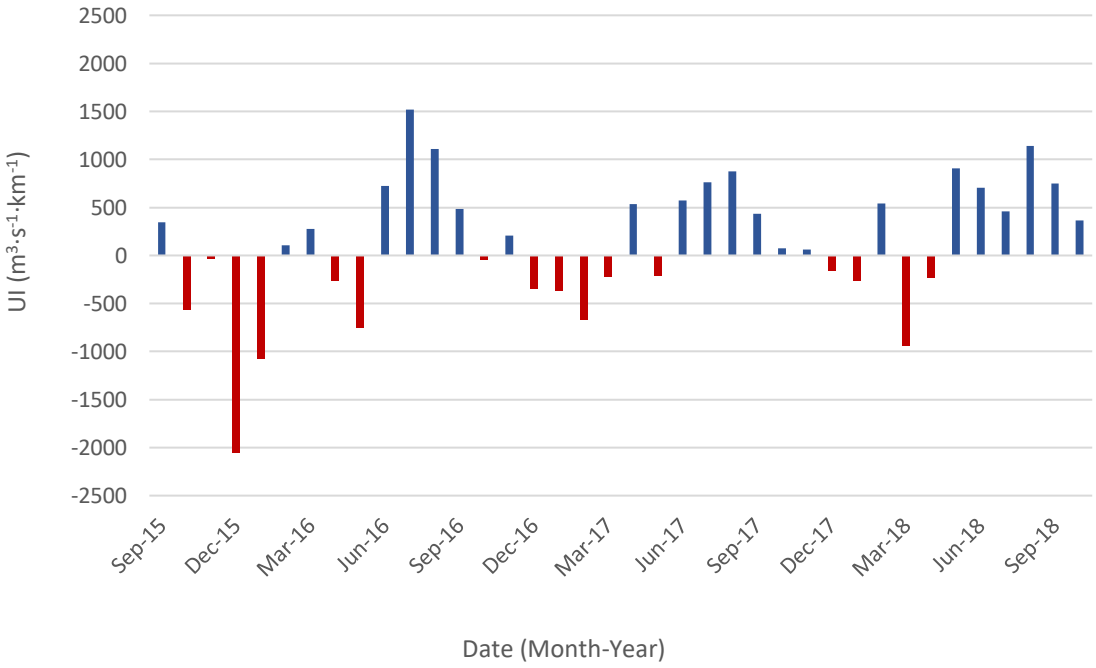

Figure 5. Time series plot of monthly mean upwelling index (UI, see text, sec. 2.8) values for the study period. Downwelling is recorded as negative UI values (red bars). Data is available from the IEO website at www.indicedeafloramiento.ieo.es.

3.1.2. Salinity

The temporal variability of salinity averaged across depths from 0 to 12 m over the duration of the three cultivation cycles at the four experimental sites is illustrated in *Figure 6*. Salinity values ranged from 31.6 to 35.6 PSU throughout the study period demonstrating a seasonal periodicity. Salinity curves display peaks toward the onset of winter and spring, with intermittent episodes during summer. Lower values and negative curves are noted throughout the rainy winter and spring seasons. Due to its proximity to freshwater discharge from the Ulla River mouth (*Figure 3*), the innermost site (InC) experienced the greatest variation in salinity throughout the study period (*Figure 6*). Cultivation cycle salinity nadirs coincide with peak mean river discharge values based on data for the Ulla and Umia rivers from MeteoGalicia and the regression model (*Figure 7*). Discharge values for both rivers ranged from 0.5 to 73.1 m^3/s peaking in late winter through spring (*Figure 7*). While the influence of freshwater runoff is most notable during winter and spring onset, a geographical salinity gradient is observed throughout the entire study period. The gradient extends from the highest values at the exterior sites to the lowest values in the interior (*Figure 6*).

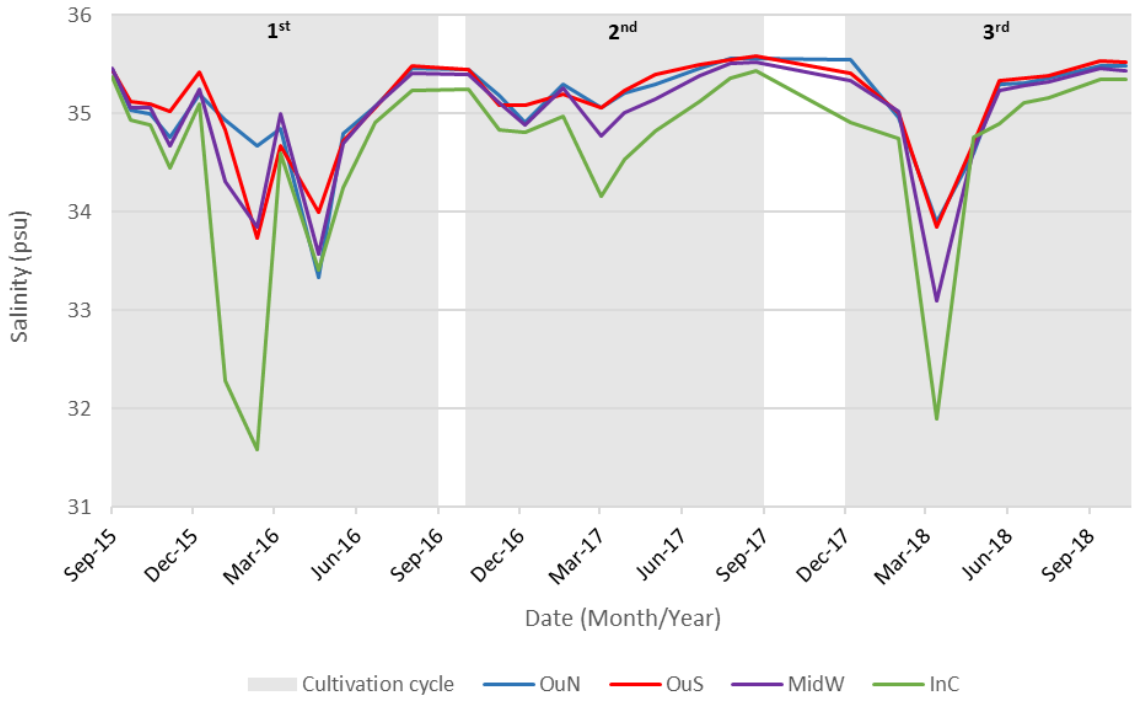

Figure 6. Time series plot demonstrating seven-day hindcasts of mean salinity values (psu) for the four experimental sites over the study period.

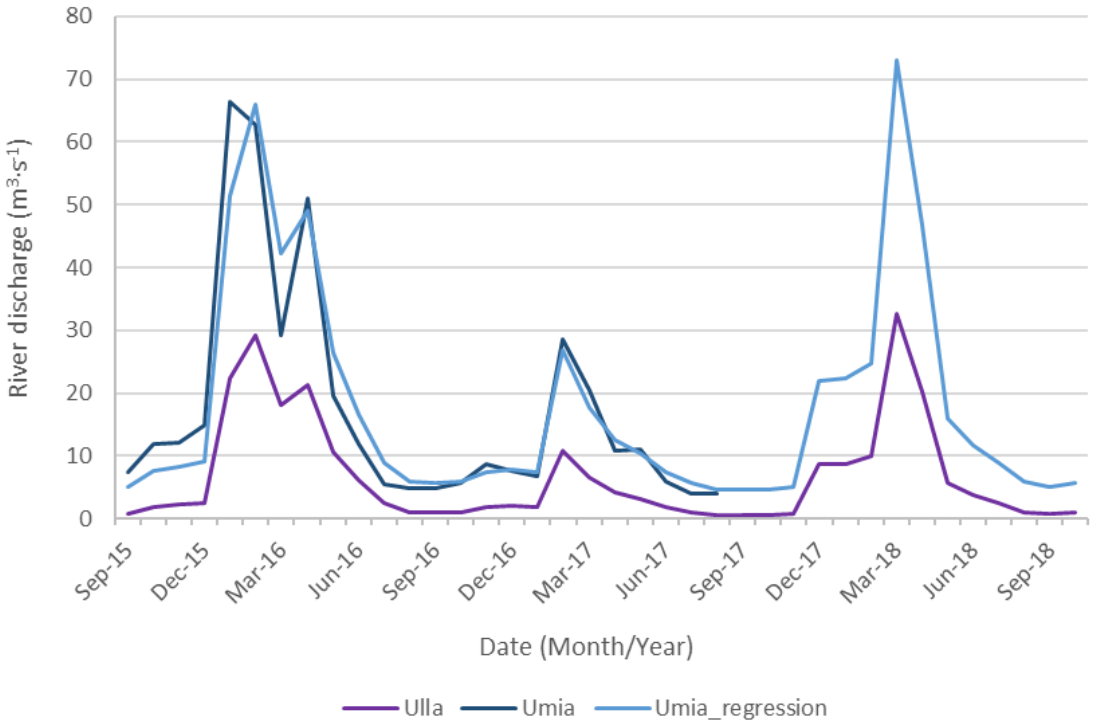

Figure 7. Time series of mean river discharge values for the Ulla and Umia over the study period provided by MeteoGalicia. MeteoGalicia data for the Umia river was unavailable from September 2017 to October 2018 and a simple regression model was used to generate the remaining Umia data (see section 2.9 for more information). Data is available from the MeteoGalicia website at www.meteogalicia.gal.

3.1.3. Food availability

The temporal variation in food availability averaged across depths from 0 to 12 m throughout the study period is represented in *Figure 8*. The food availability curve follows a cyclical pattern wherein the peaks predominately coincide with spring and autumnal phytoplankton blooms of temperate waters (Smetacek et al., 1984; Song et al., 2010; Martinez et al., 2011). The greatest values registered at the exterior sites, OuS and OuN (3.21 and 2.95 mg $m^{-2} \cdot s^{-1}$, respectively), while the lowest registered at the midcentral site (MidW = 0.10 $m^{-2} \cdot s^{-1}$), though much spatial variability is observed throughout the study period. The food availability maxima at all sites coincide with periods of positive upwelling index values observed in *Figure 5* throughout the study period, except winter of the first cultivation cycle, which displays two additional peaks during periods of downwelling. The innermost site (InC) registered large values, surpassing the remaining sites throughout much of the study period (*Figure 8*), which may reflect the bioaccumulation of phytoplankton in the interior of the ria and may also in part be attributed to organic material-rich inputs from continental runoff.

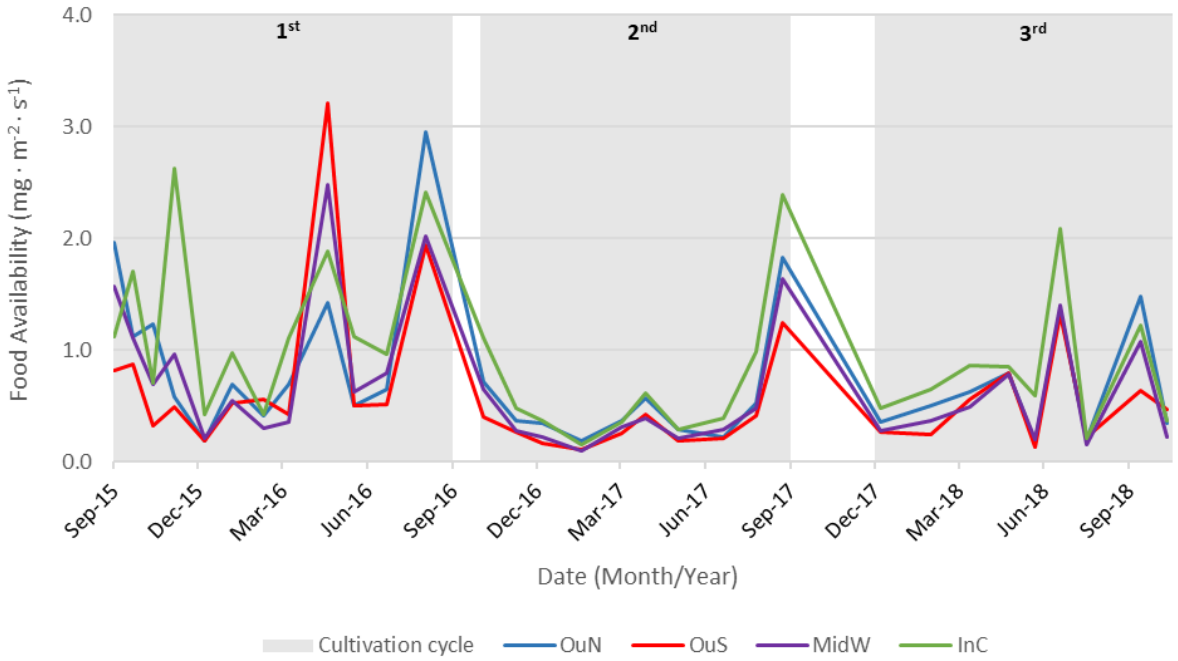

Figure 8. Time series plot of seven-day hindcasts of mean mussel food availability values ($mg \cdot m^{-2} \cdot s^{-1}$) for the four experimental sites over the study period.

3.1.4. Significant Wave Height

The temporal variation in significant wave height (H_s) during the study period is represented in *Figure 9*. Significant wave height values range from 0.12 to 1.89 m, with the maximum registering at the northern exterior site (OuN) and the minimum at the southern exterior site (OuS). The average for all sites throughout the study period was 0.52 m. Seasonal variation is exhibited by the significant wave height curves with maximum values typically peaking at the onset of spring for all sites, excepting for winter peaks observed at the southern exterior (OuS) and innermost (InC) sites during the second cultivation cycle, and the InC and midcentral (MidW) during the third cultivation cycle. Nadirs were typically observed during winter throughout the study period. Variations to this pattern are noted during winter of the first and third cultivation cycles resulting in a peak during autumn of 2015 and an early shifting in winter 2018. Despite the spatial variability in significant wave height curves, the formation of an outer-to-inner gradient is observed at seasonal transitions from autumn to winter and spring to summer, as well as over extended intervals throughout the study period (*Figure 9)*. Significant wave height peaks (*Figure 9*) also coincide with wave power curves in *Figure 10.*

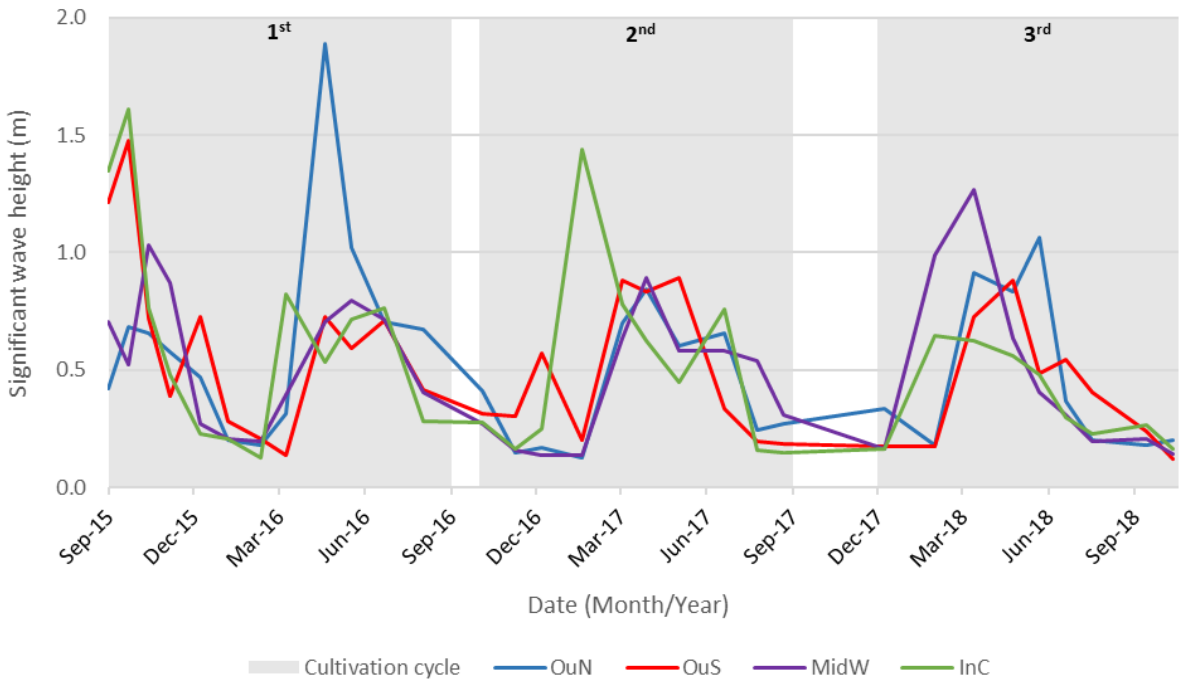

Figure 9. Time series of seven-day hindcasts of mean significant wave height values (m) for the four experimental sites during the study period.

3.1.5. Wave power

The temporal variation in total wave power (P_w) during the experimental period is represented in *Figure 10*. The annual evolution of wave power follows a seasonal pattern with maxima generally observed in spring-summer, though maxima are also noted at the onset of autumn in the first cultivation cycle. Wave power nadirs were observed during autumn, excepting the first cultivation cycle when they occurred during winter. While the greatest value registered at the northern exterior site (OuN = 23197.73 W/m), the lowest value registered at the southern exterior site (OuS = 21.34 W/m). The innermost (InC) and midcentral (MidW) sites exhibited peaks that surpassed the remaining sites during winter (InC = 14431.28 W/m) of the second cultivation cycle and at the onset of spring of the third cultivation cycle (MidW = 12479.99 W/m). The average wave power for all sites was 4610.47 W/m during the study period. Geographical patterns in wave power are observed with greater values at the exterior sites (OuN and OuS) throughout the study period for extended intervals ranging from weeks to months (*Figure 10*). Interestingly, total wave power maxima at the innermost site (InC) during the second cultivation cycle and the midcentral site (MidW) during the third cultivation cycle coincide with peak winter Ulla and Umia river discharge values, respectively (*Figure 7*). In all probability, the synoptic scales of the meteorological fields in this region that synchronize southerly winds with rain during the passing of storms, result in larger wave activity and greater runoff, therefore triggering this coincidence (Otto, 1975).

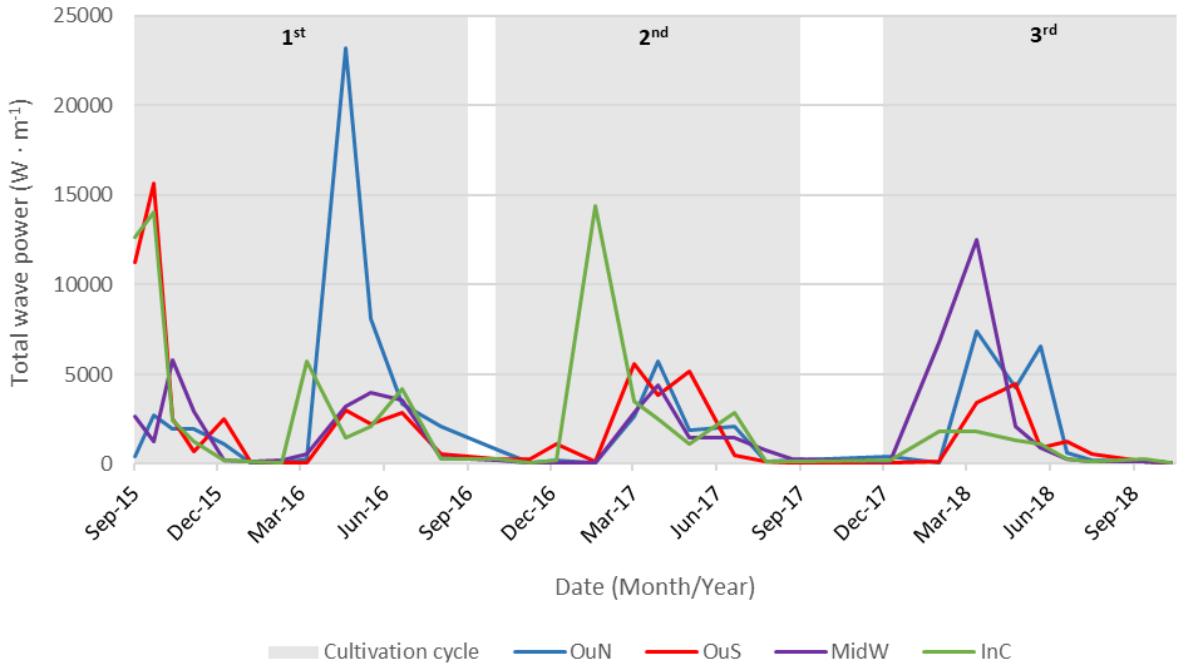

Figure 10. Time series of seven-day hindcasts of mean total wave power values for the four experimental sites during the study period.

3.2. Mussel response

It is important to note that mussel response (i.e., byssus tenacity, condition index and shell thickness index) and anemone presence scoring are illustrated in two comparisons of the factors of interest: experimental site and cultivation cycle. Although redundant, presenting cyclical and sitewide graphs provide easier and complementary comparisons of the two factors tested here. Average shell length means over the entire study period were 67.496 ± 8.255 mm, n= 46,170.

3.2.1. Biomass estimates

Weight values of the mussel-cultivated ropes throughout the experimental time were monitored *in situ* (see Material and Methods, sec. 2.7). Assuming the population density on each rope remained unchanged from initial values during each cultivation cycle, plots of the observed weight profiles *versus* theoretical maximum weight were completed to establish biomass losses. This resulted in linear models that include a 1:1 slope line provided as reference (*Figure 11*). The difference between the reference (which reflects *zero* natural mortality) and the corresponding observed slope (m) values represent an indirect measurement of the biomass losses at that site. During the first cultivation cycle (*Figure 11a*), the northern exterior (OuN), midcentral (MidW) and innermost (InC) sites exhibit steeper slopes (linear regression slopes, m= 0.79, 0.74 and 0.81, respectively) that fit well to the reference, indicating reduced losses when compared to the southern exterior site (OuS) which experienced losses at nearly double the rate (m= 0.37). The greatest losses for all sites are observed during the second cultivation

cycle (*Figure 11b*) excepting the southern exterior site (OuS), which experienced similar losses to the first cultivation cycle. By the third cultivation cycle (*Figure 11c*), the slopes steepen once more with the innermost site (InC) exhibiting the least number of losses as noted by its close fit to the reference slope (m= 0.79) while the northern exterior (OuN) site experienced the greatest losses during this period. Maximum weight values were recorded at the northern exterior site (OuN), while minimum values are observed at both the midcentral and interior sites (MidW and InC).

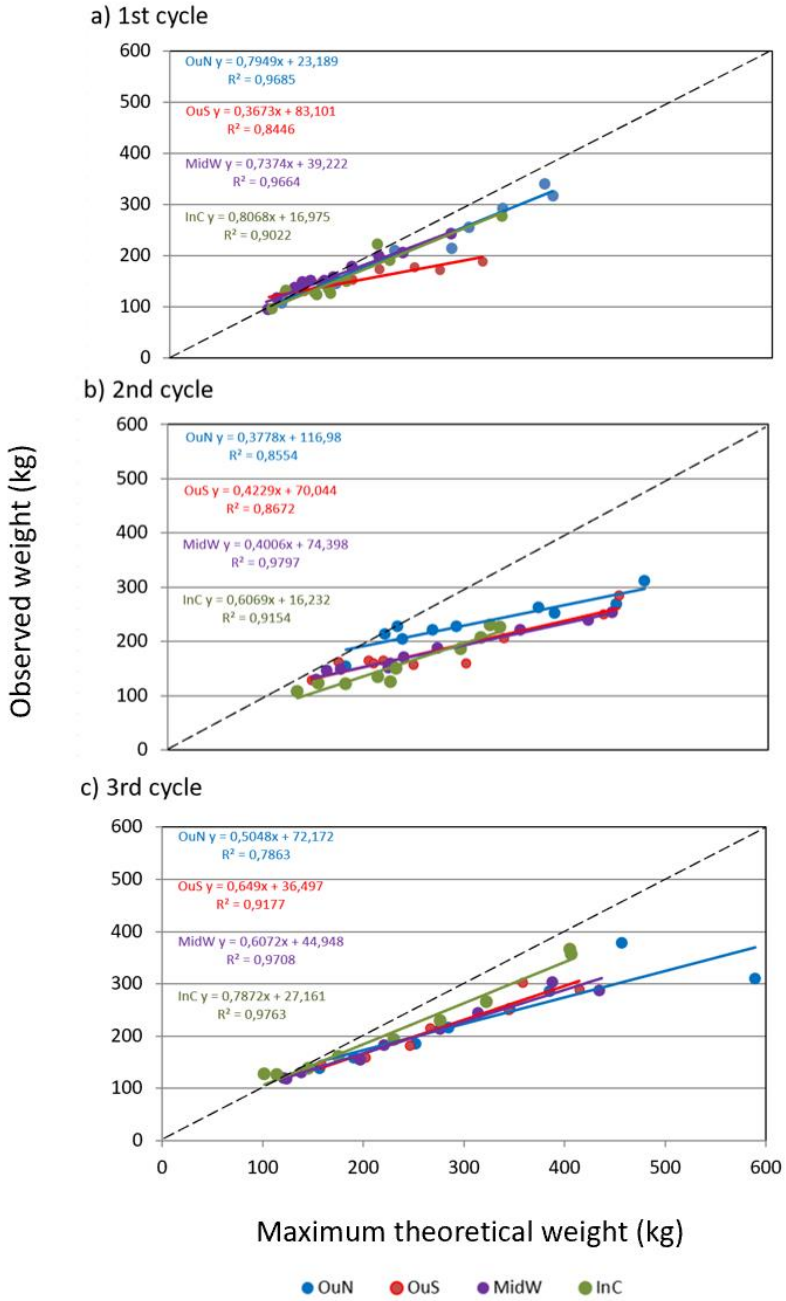

Figure 11. Cyclical trends of observed vs. theoretical maximum biomass in kg for each experimental rope. A reference line exhibiting a 1:1 relationship between the observed and theoretical weight is denoted by dash lines (- -).

Table I. ANCOVA measuring the differences between shell length, site, and cycle for tenacity, condition index, shell thickness index and anemone presence, (n=46,170). Tenacity was log-transformed. Values of p that were not significant (p ≥ 0.05) are denoted as ns.

Dependent Variable	Factor	df	*F*	p
Tenacity				
	Shell length	1	71.106	<0.001
	Site	3	21.050	<0.001
	Cycle	2	6.405	<0.01
	Site x Cycle	6	2.204	<0.05
	Error	106		
Condition Index				
	Shell length	1	10.182	<0.01
	Site	3	0.482	ns
	Cycle	2	1.871	ns
	Site x Cycle	6	0.791	ns
	Error	106		
Shell Thickness Index				
	Shell length	1	325.058	<0.001
	Site	3	2.895	<0.05
	Cycle	2	9.131	<0.001
	Site x Cycle	6	0.627	ns
	Error	106		
Anemone				
	Shell length	1	174.276	<0.001
	Site	3	53.200	<0.001
	Cycle	2	25.846	<0.001
	Site x Cycle	6	25.420	<0.001
	Error	106		

3.2.2. Tenacity

In *Table I*, ANCOVA analysis reveals that mussel tenacity was significantly influenced by shell length ($p < 0.001$), site ($p < 0.001$), cultivation cycle ($p < 0.01$) and to a lesser degree by the interaction between site and cycle ($p < 0.05$), with this model accounting for over half of the observed response ($r^2 = 0.53$). In Tukey HSD tests, significant differences were reported between the outer sites and the interior sites during the first cultivation cycle, excepting the northern exterior site (OuN) during the second cycle. Significant differences were also reported between the first cycle at the southern exterior site (OuS) and midcentral site (MidW) during the second cycle. Linear regression models with shell length displayed overall negative trends at all sites, with greater influence observed at OuS, OuN, and MidW ($r^2 = 0.50$, 0.40 and 0.44,

respectively) than InC ($r^2 = 0.23$), not shown. When ordered by cultivation cycle (*Figure 12*), shell length correlated moderately well with tenacity at all sites during the first and second cultivation cycles ($r^2 > 0.49$) but not the innermost site (InC) during the first cycle ($r^2 = 0.13$), while the weakest correlation was observed during the third cycle for all sites (*Figure 12c*). Maximum tenacity values were recorded in mussels below 60 mm during all cultivation cycles, excepting the third (*Figure 12c*). The highest tenacity values registered at the northern exterior site (OuN = 5.09 $N \cdot m^{-2}$) while the lowest was observed at the innermost site (InC = 1.27 $N \cdot m^{-2}$), representing a spatial tenacity gradient extending from the outer to inner ría (*Figure 12*). The greatest values occurred for the exterior sites during the first cultivation cycle (*Figure 13a, b*), while the interior sites peaked during the second cycle (*Figure 13c, d*). The third cultivation cycle saw a disruption of the spatial gradient with overlapping values across exterior (*Figure 13a, b*) and interior sites (*Figure 13c, d*).

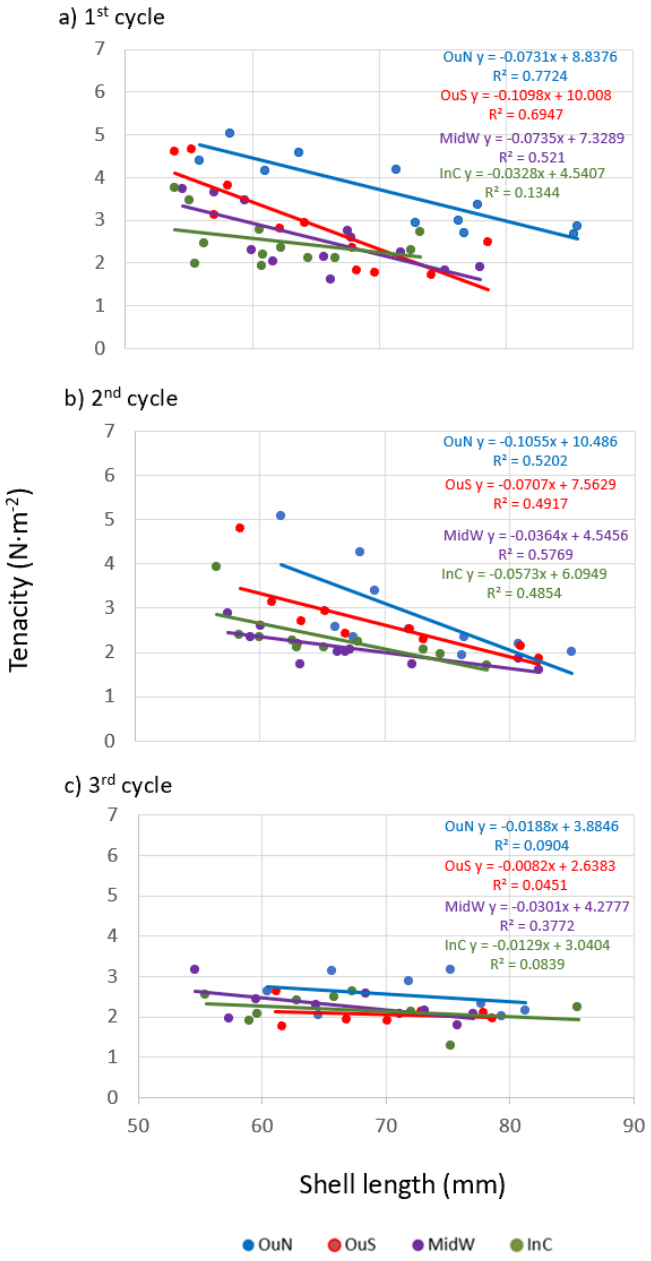

Figure 12. Cyclical trends in mussel tenacity values as a function of shell length for each experimental site.

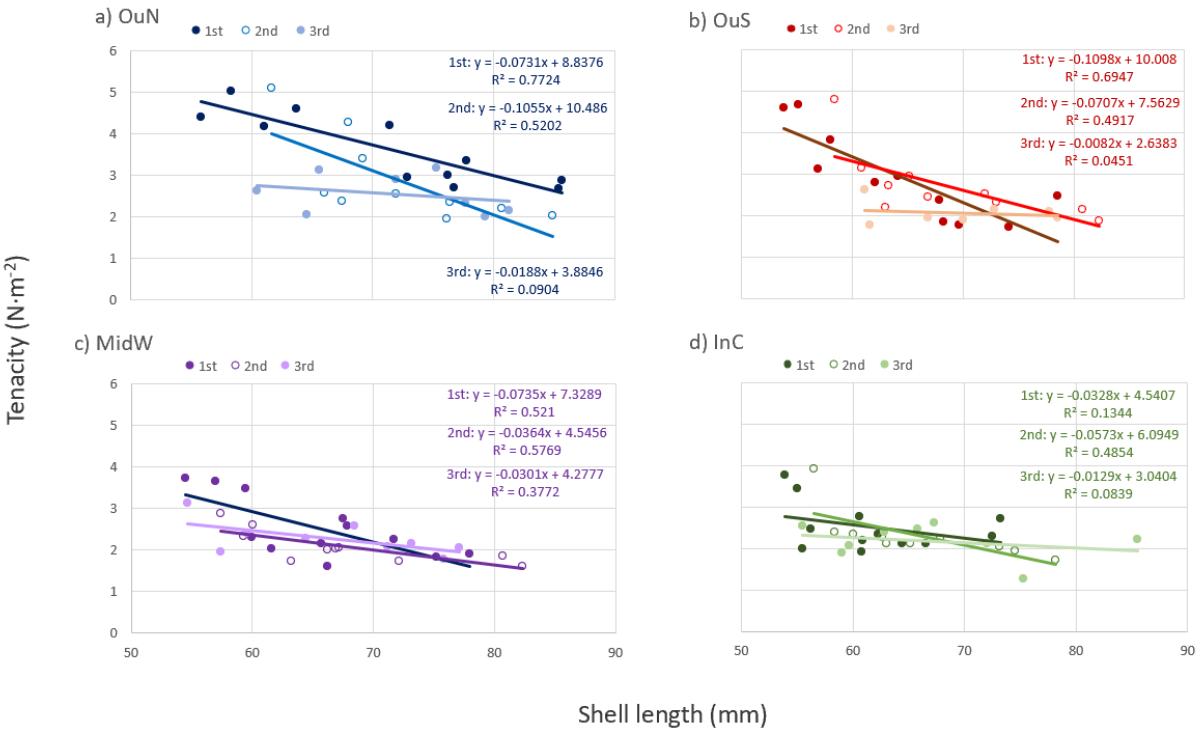

Figure 13. Sitewide trends in mussel tenacity as a function of shell length during the study period. Cultivation cycle slope lines are denoted by a dark (1st cycle), medium (2nd cycle), or light (3rd cycle) colored line.

3.2.3. Condition Index

ANCOVA analysis demonstrated that the condition index only varied significantly with shell length (*Table I*). *Figure 14* displays the linear regression models of condition index and shell length for each site over the experimental cultivation cycles. Positive trends are observed during cultivation cycles one and three for all sites (*Figure 14a*, *c*, respectively), but negative trends at the exterior sites (OuN and OuS) are noted during the second cycle (*Figure 14b*), demonstrating spatial and temporal variability of this soft tissue state index over the study period. Shell length exerted minor influences in condition index overall during the study period, with greater effects observed at midcentral and internal sites of the ría (MidW and InC, $r^2 = 0.18$ and 0.16, respectively) compared to exterior sites (OuN and OuS, $r^2 = 0.01$ and 0.04, respectively), not shown. In *Figure 15*, maximum values of condition index are observed in mussels approaching or approximately 60 mm in size during the second cycle at all sites (*Figures 15a, b, c*), excepting the innermost (InC) site (*Figure 15d*), which registered maximum values during the first cultivation cycle. The greatest condition index values registered at the northern exterior site (OuN = 35.89, *Figure 15a*) while the lowest values were seen at the southern exterior site (OuS = 11.58, *Figure 15b*). Condition Index correlated with shell length the least during the second cultivation cycle for all sites ($r^2 < 0.095$), excepting at the northern exterior site (OuN) (*Figure 15a*).

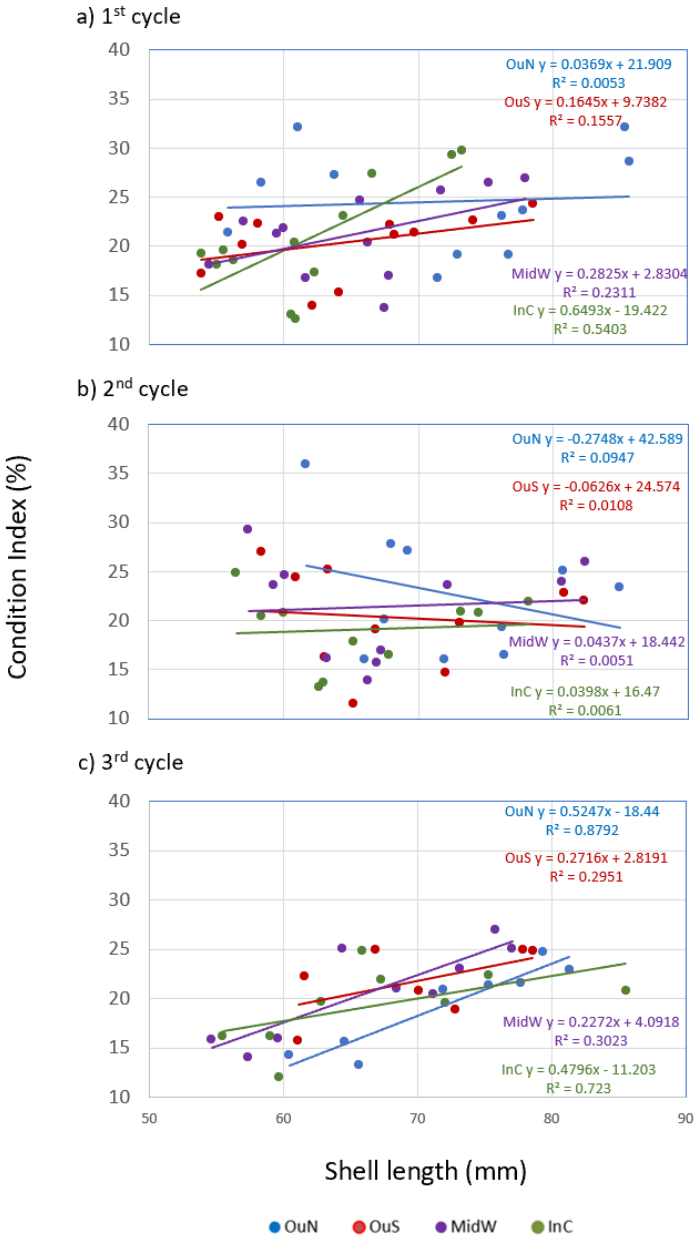

Figure 14. Cyclical trends in mussel condition index values as a function of mean shell length values per by site.

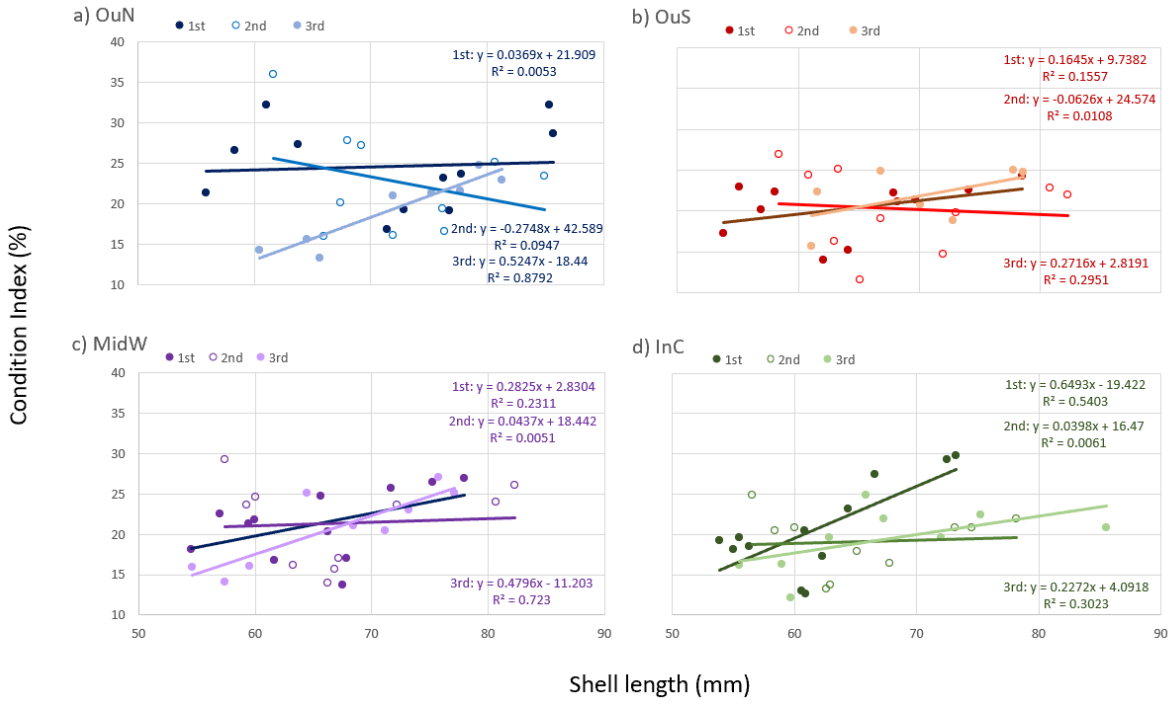

Figure 15. Sitewide trends in mussel condition index as a function of shell length during the study period. Cultivation cycle slope lines are denoted by a dark (1st cycle), medium (2nd cycle), or light (3rd cycle) colored line.

3.2.4. Shell Thickness Index

The shell thickness index demonstrated the most significant variations with shell length ($p < 0.001$), followed by cultivation cycle ($p < 0.05$) and then site ($p < 0.001$), but not the interaction between site and cycle (*Table I*) in an ANCOVA analysis, with this model accounting for a substantial portion of the observed shell thickness index response ($r^2 = 0.80$). Tukey HSD tests (not shown) established significant differences ($p < 0.01$) between the second cultivation cycle and the other cycles, whereas the northern exterior site (OuN) varied significantly ($p < 0.05$) with all sites though the greatest disparity was observed at the innermost site (InC). Between the remaining sites, shell thickness index values in the southern exterior site (OuS) and midcentral site (MidW) also varied significantly ($p < 0.05$) from the innermost site (InC). Linear regression models with shell length demonstrate positive trends for all sites during all cultivation cycles (*Figures 16*) with shell length accounting for moderate to great response variations in the shell thickness index ($r^2 = 0.45$ to 0.96). Inter-site variability is illustrated in *Figure 17*. The greatest values of shell thickness index were registered at the northern exterior site (OuN = 1.72, *Figure 17a*) while the lowest occurred at the midcentral site (MidW = 0.83, *Figure 17c*). The innermost site (InC) and the midcentral site (MidW) registered similar values during all cultivation cycles (*Figures 16, 17*). Maximum shell thickness index values were obtained in mussels exceeding 80 mm in size at all sites (*Figure 17*).

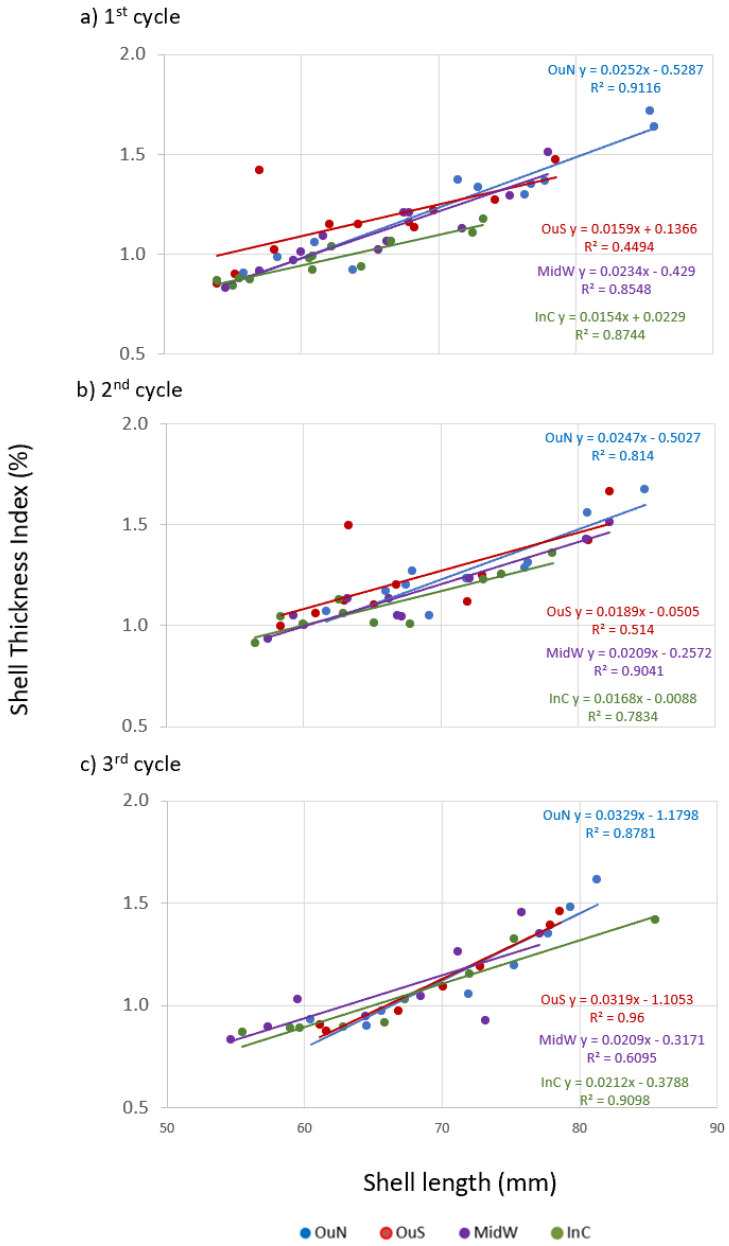

Figure 16. Cyclical trends in shell thickness index values as a function of shell length for all experimental sites.

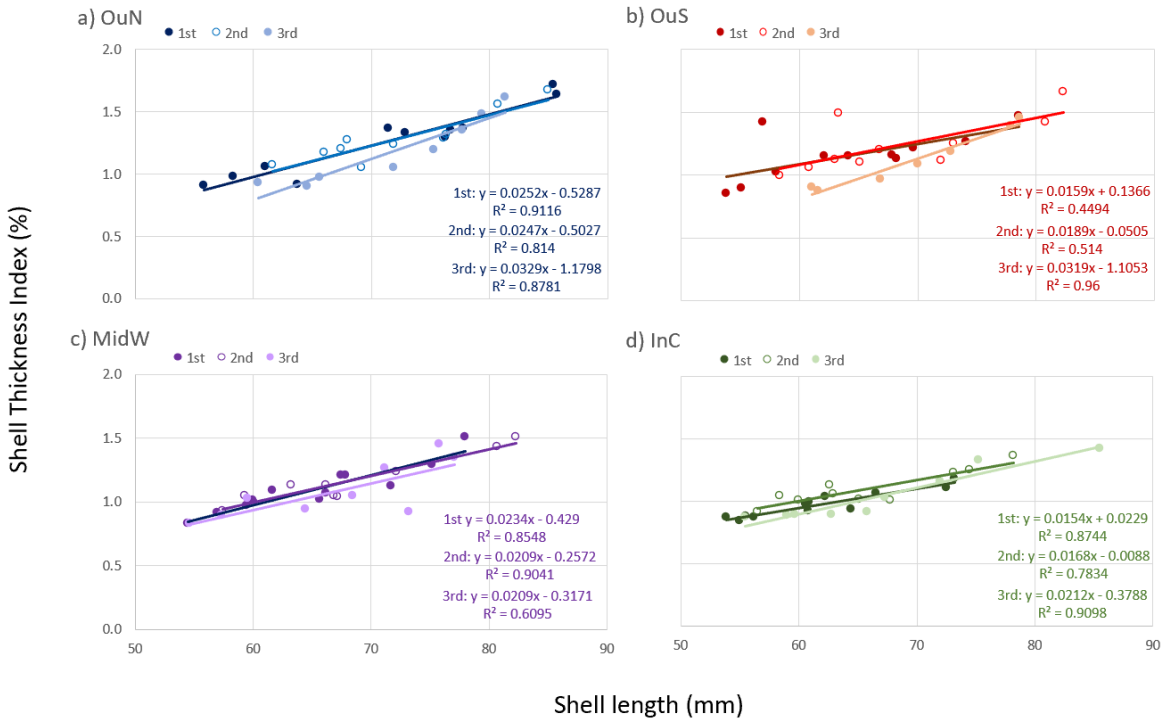

Figure 17. Sitewide trends in mussel shell thickness index as a function of shell length during the study period. Cultivation cycle slope lines are denoted by a dark (1st cycle), medium (2nd cycle), or light (3rd cycle) colored line.

3.2.5. Anemone

ANCOVA analysis (*Table I*) reveals that anemone presence was significantly influenced by shell length ($p < 0.001$), site ($p < 0.001$), cultivation cycle ($p < 0.001$) and the interaction between site and cycle ($p < 0.001$), with this model accounting for over half of the observed response ($r^2 = 0.82$). Linear regression models demonstrate positive trends between the presence of anemone and shell length (*Figure 18*, *19*) with great temporal and spatial variation. The greatest presence of anemone was registered at the southern exterior site (OuS) during the first cultivation cycle (*Figure 18a*, *19b*). During the same period, anemone presence scores at the midcentral site (MidW, *Figure 19c*) approached those of the southern exterior (OuS) while scoring at the remaining sites (*Figures 19a*, *d*) averaged <1.0 with the innermost site (InC) exhibiting the lowest presence (*Figure 19d*). Significant changes were noted the following cultivation cycle (*Figure 18b*), with scoring at the northern exterior (OuN) and innermost (InC) sites more than doubling (*Figures 19a, d*, respectively), though never reaching the levels displayed the previous year at the southern exterior (OuS) and midcentral (MidW) sites (*Figures 19b, c*, respectively). During this time, the southern exterior (OuS) displays stark decreases with the highest cycle scoring never reaching 2.5 across all shell length values (*Figure 18b*), and more attenuated decreases are noted at the midcentral (MidW) site with a slope similar to the prior cultivation cycle (*Figure 19c*). In *Figure 18c*, anemone presence has drastically decreased at all sites during the third cultivation cycle with scores failing to reach 1.5. During this period,

the greatest anemone presence scoring registered on mussels between 70 and 80 mm in length at the northern exterior (OuN, *Figure 19a*) site followed by the midcentral (MidW, *Figure 19d*) site. Most mussels below 60 mm in length at the midcentral (MidW) and innermost (InC) sites revealed little to no anemone presence (*Figures 18c, 19b, c*), a consequence of the reduced shell area available for occupation by fouling organisms.

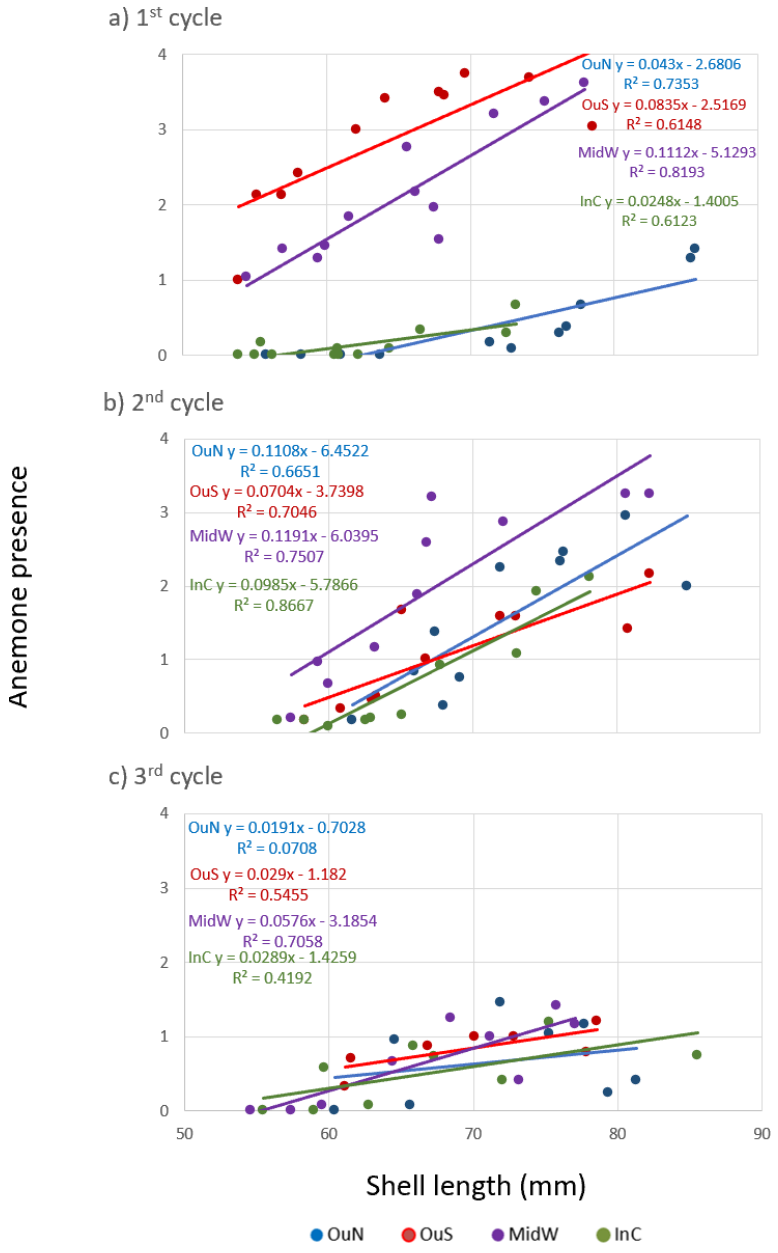

Figure 18. Cyclical trends in the epibiosis of the sea anemone Actinothoe sphyrodeta on Mytilus galloprovincialis as a function of shell length.

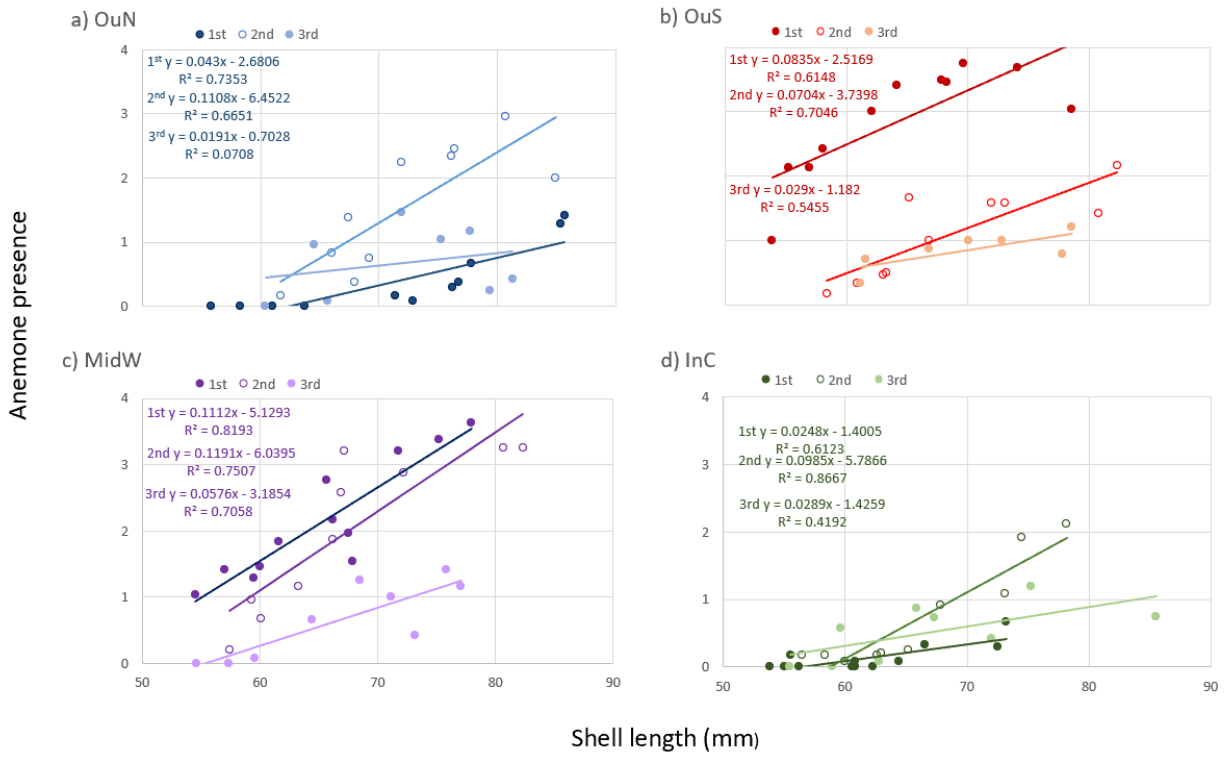

Figure 19. Sitewide trends in the epibiosis of the sea anemone Actinothoe sphyrodeta on Mytilus galloprovincialis as a function of shell length during the study period. Cultivation cycle slope lines are denoted by a dark (1st cycle), medium (2nd cycle), or light (3rd cycle) colored line.

As reported above, anemone presence varied by cultivation cycle and this interannual variation is also illustrated in linear regression models between mussel biological responses to anemone presence in *Figures 20, 21 and 22*.

Figure 20 demonstrates the overall negative influence of anemone presence on mussel tenacity for all sites. During the first cycle, the sites with the greatest anemone presence, the southern exterior (OuS) and midcentral (MidW), demonstrate the greatest descents in mussel tenacity (*Figure 20b* and *20c*, respectively) with greater modulation at OuS than MidW (r^2 = 0.79 and 0.59, respectively). The following cycle, when anemone presence increased at the northern exterior (OuN) and innermost (InC) sites (*Figure 20a and 20d*) while decreasing at its previous strongholds (OuS and MidW), the influence of sea anemone on tenacity increased at OuN, MidW and InC (r^2 = 0.68, 0.59 and 0.26, respectively) while decreasing at OuS (r^2 = 0.37). The third cycle displayed the lowest influence of anemone presence on tenacity at all sites (r^2 < 0.19) excepting the southern exterior (OuS, r^2 = 0.44).

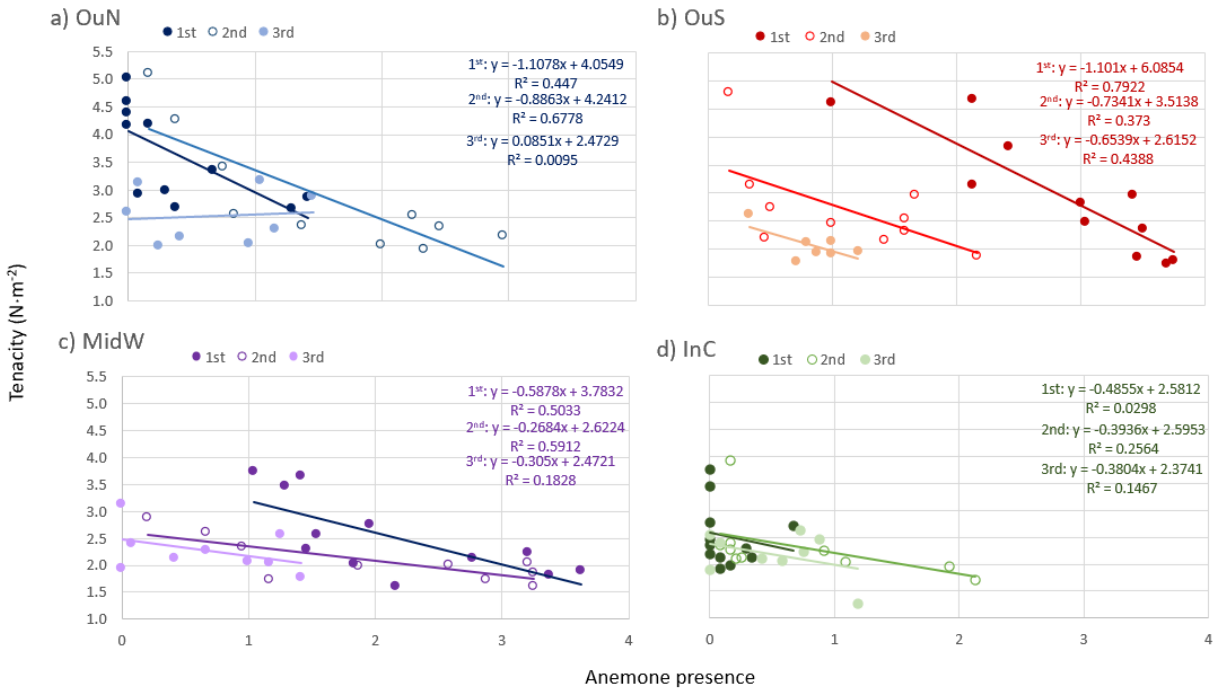

Figure 20. Sitewide trends in mussel tenacity as a function of epibiosis by the sea anemone Actinothoe sphyrodeta during the study period. Cultivation cycle slope lines are denoted by a dark (1st cycle), medium (2nd cycle), or light (3rd cycle) colored line.

The response between mussel condition index and anemone presence during the study period is displayed in *Figure 21*. Condition index correlates positively with anemone presence during the first cycle at all sites, though this correlation is weaker at the exterior sites (*Figure 21a* and 21*b*) than the interior sites (*Figure 21c* and 21*d*). A reverse pattern is observed during the second cycle with condition index at the exterior (OuN and OuS) and midcentral (MidW) sites (*Figures 21a, b, c*) negatively correlating with anemone presence, excepting the innermost (InC) site (*Figure 21d*), which displayed positive correlations during all cycles. During the third cycle, a positive relationship is exhibited again at all sites, accounting for 26 to 34% of condition index variability at the OuN, OuS and InC sites (r^2 = 0.26, 0.34 and 0.33, respectively) while accounting for 64% at the MidW site.

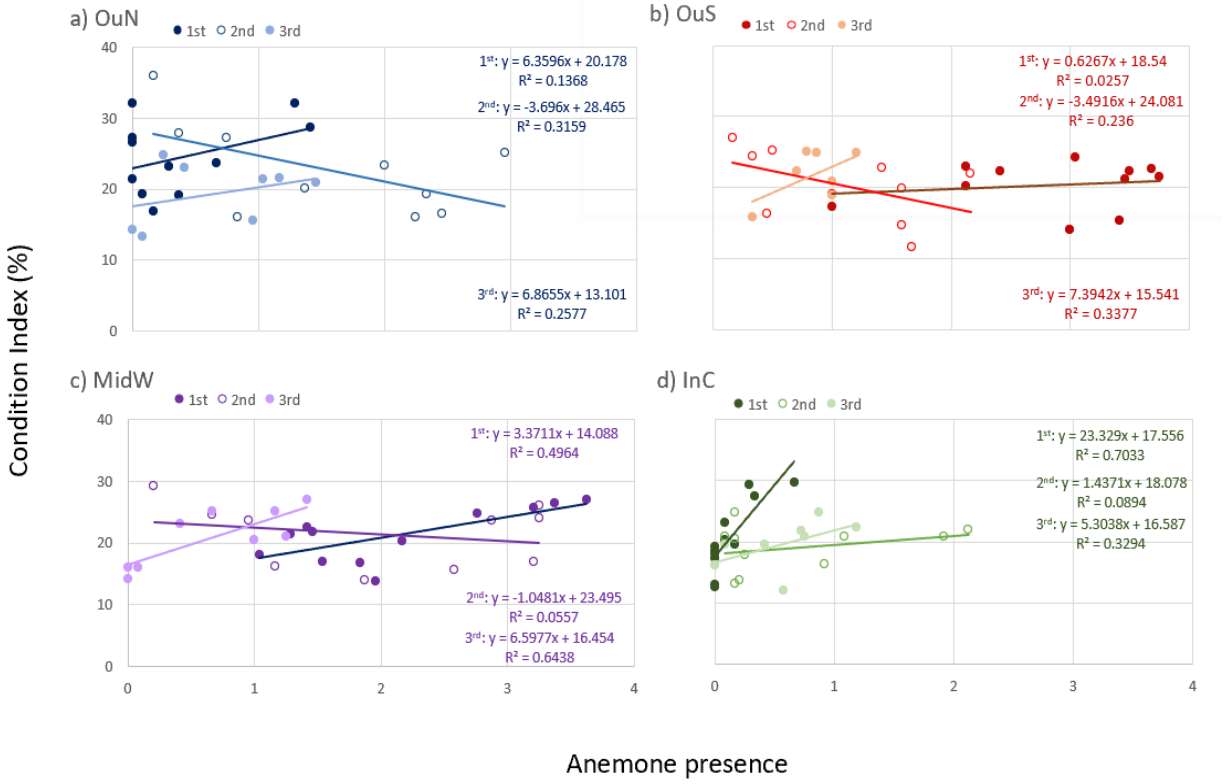

Figure 21. Sitewide trends in mussel condition index as a function of epibiosis by the sea anemone Actinothoe sphyrodeta during the study period. Cultivation cycle slope lines are denoted by a dark (1st cycle), medium (2nd cycle), or light (3rd cycle) colored line.

Figure 22 illustrates the positive correlation of anemone presence on mussel shell thickness during the study period. The northern exterior (OuN) site exhibited STI values > 1.5 during all cycles with varied anemone presence scoring of 0 to 3 (*Figure 22a*). While STI maxima at the southern exterior (OuS) site (*Figure 22b*) approached those of OuN, they peaked during the second cycle when anemone presence had diminished at OuS (anemone presence score < 3). The midcentral (MidW) site exhibited peaks during the first and second cycles when anemone presence scored higher (*Figure 22c*). Maxima values for the innermost (InC) site never reached those of the remaining sites and occurred during the second and third cycles when anemone presence had peaked there (*Figure 22d*).

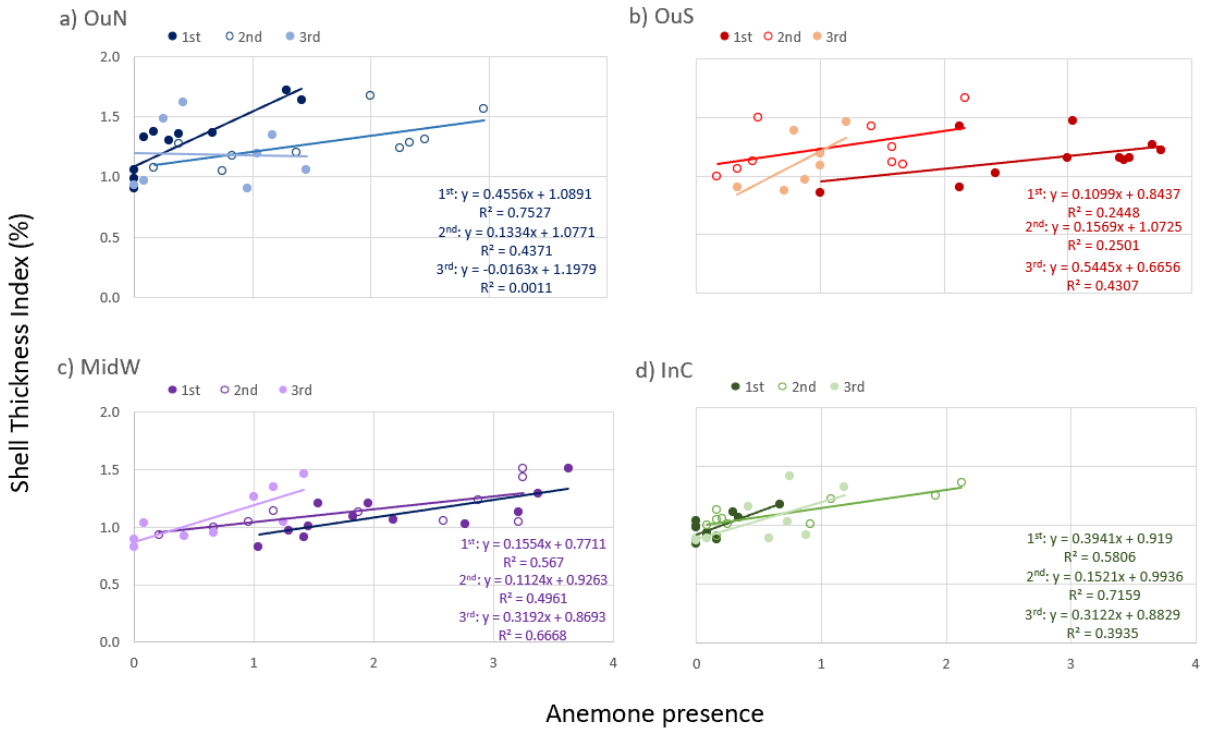

Figure 22. Sitewide trends in mussel shell thickness index as a function of epibiosis by the sea anemone Actinothoe sphyrodeta during the study period. Cultivation cycle slope lines are denoted by a dark (1st cycle), medium (2nd cycle), or light (3rd cycle) colored line.

3.2.6. Multiple Regression Analysis

Multiple regression analysis models were applied to evaluate the variability of raft-cultivated mussel responses to site-mediated environmental parameters for each experimental site (see section 2.9. in Materials and Methods for the temporal span of lagged averages considered).

A multiple regression model consisting of anemone presence, longitude, temperature in 7-day hindcasts (T_7), and significant wave height at 15-day hindcasts (H_s_15) explained nearly 36% of the variation in mussel byssus tenacity (adjusted r^2= 0.362), with anemone presence exerting the most significant influence (*Table II*). As demonstrated in *Table II*, tenacity is differentially impacted by the factors making up this model whereby tenacity increases with temperature and significant wave height, while decreasing with longitude and epibiosis by the sea anemone. For mussel condition index, 43% of the variation at all sites (adjusted r^2= 0.426) is explained by a multiple regression model consisting of food availability lags at 45 days (FA_45), salinity at 7-day lags (S_7), longitude (position along the outer-inner axis of the Ría de Arousa), and temperature at 15-day lags (T_15) with the most significant factor being FA_45. Condition index increases with food availability, salinity and temperature, while decreasing with longitude (*Table II*). Multiple regression analyses revealed that anemone presence and food availability at 45-day lags correlated positively while longitude correlated negatively with shell

thickness index (*Table II*), explaining 29% of the variation at all sites (adjusted r^2= 0.286). The anemone presence exerts the most significant influence ($p < 0.001$) in this model (*Table II*).

Longitude, the geographic coordinate that defines the horizontal displacement from the prime meridian (negative westwards), was used here to test potential spatial effects of cultivation rafts along the outer-inner axis of the Ría de Arousa. Interestingly, longitude exhibited a negative correlation in all cases, indicating that mussels were characterized by significantly lower byssus tenacity, condition index and shell thickness index values as you move inshore.

Table II. Multiple regression analyses between longitude, anemone, and all environmental factors resulted in the following mussel response models. Values of p that were greatly significant are denoted as (p ≤ 0.001). Each environmental parameter is denoted by the applicable temporal lag period. Food availability and wave height are respectively abbreviated as "FA" and "H_s".

Mussel response	Variable	Non-standardized β coefficient	STD	t	p
Tenacity					
	(Constant)	-49.153	9.486	-5.182	< 0.001
	Anemone	-0.321	0.056	-5.705	<0.001
	Longitude	-5.515	1.062	-5.192	<0.001
	Temperature 7	0.182	0.045	3.992	<0.001
	H_s 15	0.499	0.163	3.068	<0.01
	Model		r^2	*F*	p
			0.362	17.709	< 0.001
Condition Index					
	(Constant)	-217.054	53.377	-4.066	< 0.001
	FA 45	6.752	1.051	6.422	< 0.001
	Salinity 7	1.203	0.571	2.107	<0.05
	Longitude	-20.219	6.230	-3.245	<0.01
	Temperature 15	0.737	0.308	2.388	<0.05
	Model		r^2	*F*	p
			0.445	22.874	< 0.001
Shell Thickness Index					
	(Constant)	-9.587	2.688	-3.566	< 0.001
	Anemone	0.070	0.016	4.442	< 0.001
	Longitude	-1.187	0.302	-3.931	< 0.001
	FA 15	0.104	0.037	2.844	<0.01
	Model		r^2	*F*	p
			0.286	16.776	< 0.001

To illustrate the impact of each mussel response, simple linear regression models were generated (*Figures 23, 24 and 25*) selecting the most significant parameter for each model indicated in *Table II*. In contrast to cyclical linear regression models previously presented in this study, the following graphs exemplify sitewide relationships over all cultivation cycles.

Figure 23 illustrates the negative correlations between mussel tenacity and anemone presence at all sites, displaying a spatial gradient from outer and inner ría when anemone presence is low. The northern exterior site (OuN) exhibits a steeper slope than the remaining sites, indicating a greater decline in tenacity with anemone epibiosis. An ANCOVA analysis (*Table III*) confirmed that tenacity varied significantly with anemone presence ($p < 0.001$) and site (longitude, $p < 0.001$), revealing the outer-to-inner ría gradient previously seen in *Figure 12a* and *12b*.

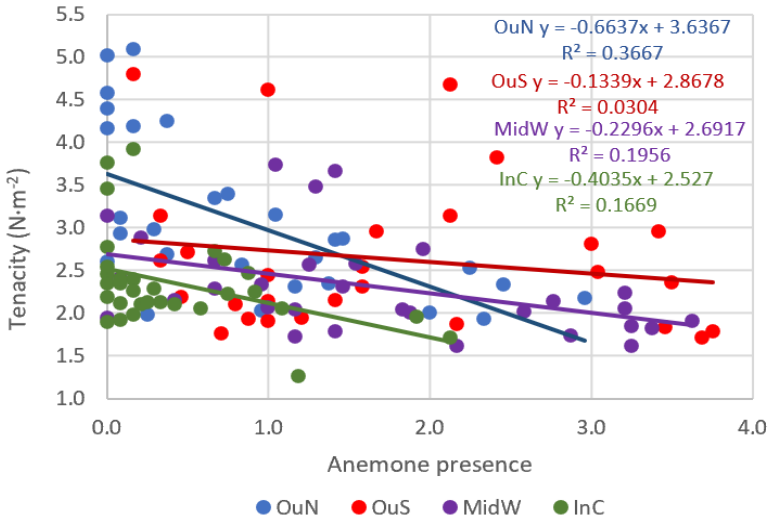

Figure 23. Sitewide trends in mussel tenacity as a function of anemone presence for all cultivation cycles.

Table III. ANCOVA measuring the differences between site and the most significant parameter for each respective mussel response (as indicated by the multiple regression analysis in Table 2): mussel tenacity, condition index and shell thickness index (n=46,170). Tenacity was log-transformed prior to the analysis. Food Availability at a 45-day lag is denoted as "FA 45".

Mussel response	Factor	df	*F*	p
Byssus tenacity				
	Anemone	1	21.532	<0.001
	Site	3	8.380	<0.001
	Error	114		
Condition Index				
	FA 45	1	59.775	<0.001
	Site	3	6.882	<0.001
	Error	114		
Shell Thickness Index				
	Anemone	1	28.392	<0.001
	Site	3	7.697	<0.001
	Error	114		

Figure 24 demonstrates positive correlations between mussel condition index and food availability at all sites. Despite similar increases in food availability, the innermost site (InC) displays much lower condition index values than the remaining sites. Much overlap between the southern exterior (OuS) and midcentral (MidW) sites is also noted (*Figure 24*) despite differing hydrodynamic stress conditions (*Figures 9, 10*). An ANCOVA analysis of food availability at 45-day lags and site (longitude) (*Table III*) confirmed their significant impact ($p < 0.001$) on condition index.

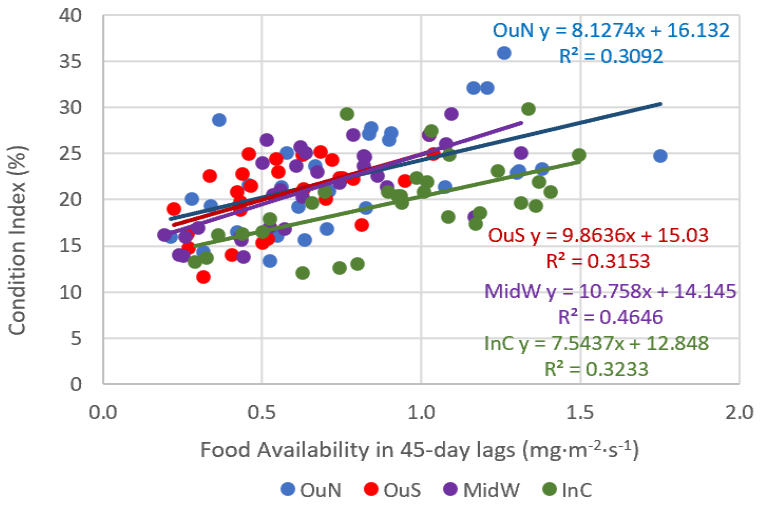

Figure 24. Sitewide trends in mussel condition index as a function of 45-day increments of food availability for all cultivation cycles.

Figure 25 illustrates the positive correlations between mussel shell thickness index and anemone presence at all sites, revealing a spatial outer-to-inner ría gradient (as previously seen in *Figure 14*) when the anemone is absent. The innermost site (InC) displays a slightly steeper slope despite its location in relatively sheltered conditions (*Figures 9, 10*), indicating a greater increase in shell thickness index with anemone epibiosis. ANCOVA analysis (*Table III*) confirmed the significant influence that anemone presence ($p < 0.001$) and site (longitude, $p < 0.001$) exert on shell thickness index.

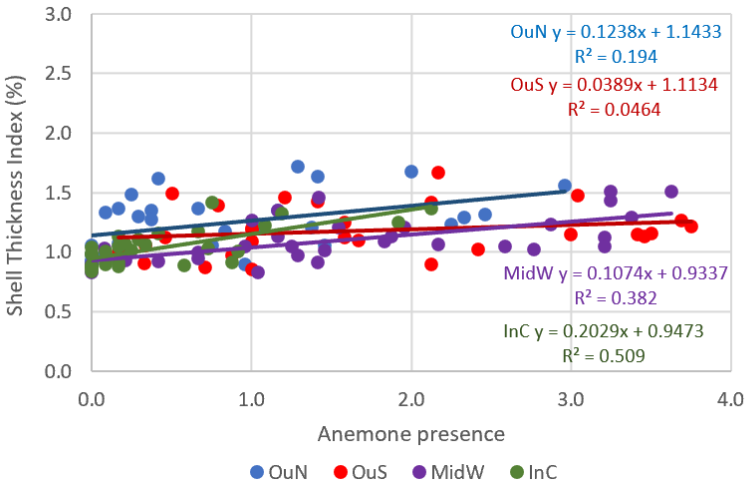

Figure 25. Sitewide trends in mussel shell thickness index as a function of anemone presence for all cultivation cycles.

4. DISCUSSION

Environmental parameters followed seasonal variation at all sites throughout the study period (*Figures 4, 6, 8, 9, 10*). A spatial gradient was observed in all environmental parameters, excepting food availability (*Figure 8*), of varying durations and intervals. Temperature displayed alternating colder outer-to-inner and inner-to-outer gradients on time scales of several months (*Figure 4*). Wave power and significant wave height also displayed a calmer inner-to-outer gradient over multiple months (*Figures 9, 10*), whereas this same spatial gradient remained constant throughout nearly all the study period for salinity (*Figure 6*) with brackish waters inshore. Prolonged periods of these geographical patterns resulted in raft-cultivated mussels developing in very distinct environmental conditions that likely affect mussel responses throughout the cultivation cycles. The exterior sites (OuN and OuS) are generally characterized by greater saline (*Figure 6*) and hydrodynamic stress (*Figures 9, 10*) conditions than the midcentral (MidW) and interior (InC) sites, whereas the latter is influenced by freshwater discharges from the Ulla River. The heterogeneous environments that characterize the Ría de Arousa may modulate energetic tradeoffs that mussels access, allocating energy to very distinct vital functions such as fitness and protective strategies during cultivation at the selected experimental sites.

The environmental gradients are also reflected in the spatial and temporal variation in observed mussel dislodgements or biomass losses. The greatest observed biomass values occurred during the first cultivation cycle for all sites (*Figure 11*), excepting the southern exterior (OuS) site, whose losses during this period coincide with the greatest incidence of epibiosis by the sea anemone *Actinothoe sphyrodeta* (*Figures 18a, 19b*). Similar levels of anemone epibiosis were detected at the southern exterior (OuS) and midcentral (MidW) sites during the first cultivation cycle (*Figures 19b, c*, respectively) albeit with different biomass losses. This disparity is likely because the MidW site is subjected to less hydrodynamic stress (i.e., wave power and significant wave height) than the outer more exposed southern (OuS) site (*Figures 9, 10*). During autumn of the first cultivation cycle, the OuS registered the lowest food availability concentration (*Figure 8*) while simultaneously subjected to some of the greatest hydrodynamic stress values (*Figures 9, 10*), creating an energetically stressful period that resulted in synergistic dislodgement effects when coupled with high anemone epibiosis (*Figure 18a*) during this time and throughout the remainder of the first cycle. By the second cultivation cycle, the spatial distribution of anemone epibiosis had expanded to the northern exterior (OuN) and innermost (InC) sites resulting in similar dislodgement slopes across all sites (*Figure 11*), except the InC due to a lower anemone presence (*Figure 18b*). The third cultivation cycle saw a reduction in anemone epibiosis at all sites (*Figure 18c*) and similar dislodgement rates at all sites (*Figure 11*) except the innermost (InC), which coincided again with the lowest anemone presence during this cycle (*Figure 19d*). These results represent a critical combination of abiotic (i.e., hydrodynamic flow regimes) and biotic (i.e., biofouling) factors that likely explain observed changes in the raft-cultivated mussel biomass. Previous biofouling by *A. sphyrodeta* resulting in significant dislodgements were recorded at these sites with observed biomass losses

of up to 14% and 40% at the MidW and OuS sites, respectively (Babarro et al., 2019). The interannual epibiosis variability by the marine anemone *A. sphyrodeta* displayed a fluctuating spatial distribution at all experimental sites (*Figure 18*). While anemone epibiosis correlated positively with mussel shell length due to the continuous increase in substrate area (mussel shell) for the anemone to attach to (*Figures 18, 19*), the highest incidence of epibiosis was not observed on the largest mussels (*Figure 25*). Mussel shell length means over the three cultivation cycles also display an outer-to-inner gradient with the greatest values reported at the exterior sites while the lowest occurred in the interior (average shell length means, OuN = 71.85, OuS = 67.25, MidW = 66.50 and InC = 64.64 mm), not shown. Despite the largest shell length values registering at the OuN site, the highest incident of anemone epibiosis registered at the OuS site during the first cultivation cycle (*Figure 18a*). Subsequent cultivation cycles demonstrate an expansion northward and inshore followed by a retreat at all sites (*Figure 18b, c*). The spatial distribution and ensuing diminished anemone presence coincide with an ascent in annual upwelling index values (*Figure 26*), yet additional studies would need to be performed to determine the role of upwelling, if any. Consequently, the synergistic effects of hydrodynamic stress and anemone epibiosis display fatal consequences for raft-cultivated mussels resulting in acute economic losses.

Following hydrodynamic trends (*Figures 9, 10*), protective tissues (i.e., shell thickness and byssus attachment strength) displayed a spatial gradient with the lowest values registering at the interior sites while the greatest values are observed at the exterior, more oceanic sites (*Figures 16, 12,* respectively). This gradient was previously observed in the Rías Baixas by Babarro and Carrington (2011, 2013) and Babarro et al. (2019, 2020). The spatial variability of byssus tenacity corresponded to greater values at the northern exterior (OuN) site followed by the southern exterior (OuS) while values were comparable at the midcentral (MidW) and innermost (InC) sites (*Figure 13*). While byssus tenacity correlates negatively with shell length throughout the study period (following the known inverse relationship of mussel size and tenacity), the overall tenacity values also decrease with each successive cultivation cycle resulting in the recording of the lowest maxima values at all sites during the last cycle (*Figure 12c*). In contrast, shell thickness index values increase with shell length, but as with tenacity, also exhibited lower values during the third cultivation cycle (*Figure 16c*). Previous studies in cultivated mussels normalized to a standard size of 60 mm indicated a seasonal effect in shell thickness index, which was not studied here (Babarro et al., 2020). Though the protective tissue patterns described in the present study coincide with successive wave power and significant wave height peak maxima values decreasing over the study period (*Figures 9, 10*), multiple regression analyses indicate that biofouling by *A. sphyrodeta* holds the greatest influence in protective tissue models (*Tables II, III*). Indeed, the two protective tissues secreted by mussels throughout their life cycle (i.e., byssus strength and calcium carbonate shell) are greatly characterized by changes in the presence of key fouling organisms like the marine anemone *A. sphyrodeta*. Additional studies examining mussel response parameters over longer periods may be helpful to further elucidate additional synergistic effects with anemone influence or other

fouling species of interest.

The northern exterior site (OuN) exhibits the greatest values across all mussel response parameters studied here during nearly every cultivation cycle. An exception to that trend was observed during the third cultivation cycle (*Figure 14c*), when the greatest condition index value registered at the midcentral site (MidW). Despite the spatial variation in hydrodynamic regime between the MidW and southern exterior (OuS) sites (*Figures 9, 10)*, overlapping condition index values are observed at these sites (*Figure 15c, b*, respectively). Moreover, although the exterior sites (OuN and OuS) register the greatest food availability values (*Figure 8*), condition index curves display alternating interannual trends (*Figure 14a, b*, respectively). These discrepancies between the influence of environmental factors on mussel condition index have been previously observed in the Ría de Arousa (Babarro and Reiriz, 2010; Babarro and Carrington, 2011; Babarro et al., 2020), and are attributed to endogenous rhythms related to sexual cycle and spawning events (Babarro and Reiriz, 2010). Spawning is an energetically demanding annual event (Zardi et al., 2007) that can result in reduced byssus tenacity and diminished food absorption efficiency despite optimum conditions (Babarro and Reiriz, 2010), engendering energetically weaker mussels during this stressful period. Put another way, in a greater hydrodynamic environment, spawning mussels are forced to prioritize metabolism toward protective and reproductive tissues resulting in less energy available for the growth of other soft tissues. In the present study, raft-cultivated mussels at the exterior sites (OuN and OuS) are subject to greater hydrodynamic stress conditions resulting in lower condition index values than the sheltered midcentral (MidW) and interior (InC) sites when these energetic tradeoffs occur. While abiotic factors are not as influential in predicting mussel condition index, food availability was highly significant in the multiple regression analysis (*Table II*), which likely relates to the organism's ability to meet overall metabolic needs.

The application of multiday lags in abiotic factors was valuable in examining raft-cultivated mussel biological responses that operate on diverse temporal scales. The temporal property of the mussel responses was reflected in the corresponding time lags of the environmental parameters indicated in the multiple regression models (*Table II*). Shorter lags of temperature and significant wave height (7-day and 15-day, respectively) modulated mussel tenacity and, by extension, the byssus since the former is determined by the force required to overcome the attachment strength of the latter (*Equation 1*). While temperature was more statistically significant ($p < 0.001$) than significant wave height (< 0.01), the short time scales of both abiotic drivers agree with that of byssus, which is secreted in minutes and decays over multiple weeks (Bell and Gosline, 1996). Although shorter lags of temperature and salinity (15-day and 7-day, respectively) contributed to the variability seen in mussel condition index (*Table II*), these factors were not as significant ($p < 0.05$) as the longest lag of food availability (45-day, $p < 0.001$). Since condition index is an estimate of the nutritional and gonadal status of the soft tissue, which is greatly influenced by endogenous cycles that operate on yearly time scales (Babarro and Carrington, 2011), the longer lag in food availability agrees with the temporal

scale of this response. In contrast, mussel shell thickness index was influenced by a shorter lag of food availability (15-day), though this was the least significant factor in the multiple regression model (*Table II*). Shell thickness index is an approximation for shell growth, which is continuous and energy-intensive (Gardner and Thomas, 1987), and consequently, the shorter lag in food availability is seemingly in agreement with this response as well. The abiotic factors discussed here all correlated significantly ($p < 0.05$), often very significantly ($p < 0.001$), and exemplify short and long-term drivers uniquely influencing each respective mussel response model during the experimental period. The multiple regression models reveal the deterministic effect imparted by these drivers on raft-cultivated mussel response, but there may be additional abiotic factors (e.g., water pH, turbulence, biofouling by additional epibionts, etc.) that warrant further investigation to continue reducing the possibility of any stochastic effects. The findings from the application of temporal lags in abiotic factors in the present study demonstrate the relevance and need for its employment in future studies.

Raft-cultivated mussel biological responses are modulated by biotic and abiotic factors reflecting distinct environmental conditions throughout the Ría de Arousa. The present work follows previous studies (Babarro et al., 2019; Babarro et al., 2020) in providing additional information on raft-cultivated mussel biological responses and epibiosis by the marine anemone *A. sphyrodeta* in the study area. The plasticity of *Mytilus* byssus is hydrodynamically driven, capable of switching to quinone-derived crosslinks in their proteins under higher flow regimes (McDowell et al., 1999), and the strength of *Mytilus galloprovincialis* in particular may be attributed to the additional histidine residues in the byssus flanking domains resulting in the formation of additional metal chelation crosslinks (Lucas et al., 2002). These structural components of *Mytilus* byssus protein provide greater stability and integrity (Lucas et al., 2002) but are sensitive to microplastics (Green et al., 2019) and changes in temperature and pH meaning that ocean pollution, acidification and warming is likely to result in weaker byssus (Carrington et al., 2015). With the advent of harsher climate change conditions predicted in the coming decades (IPCC, 2022), mussel biological responses are likely to depart from those reported here. Given the disproportionate amount of mussel cultivation rafts in the Ría de Arousa (Mexillón de Galicia, 2023a), further investigations into the effects of environmental parameters and epibiosis on these mussel populations would be helpful in generating long-term mussel biological response data that when coupled with mussel dislodgement models (Carrington et al., 2009; Babarro et al., 2020) may help specify optimum areas of cultivation in the Ría de Arousa.

5. CONCLUSION

The biological responses studied here in raft-cultivated mussels display tradeoffs in energetic allocations operating over divergent time and spatial scales. Mussels at sites

characterized by high-energy regimes exhibit changes in energy allocations when subjected to additional environmental stressors such as *A. sphyrodeta* epibiont blooms (biotic factor) and lower food concentrations (abiotic factor), exerting a bottom-up control that leads to greater dislodgements or biomass losses and economic losses.

Despite a dichotomous hydrodynamic environment between the outer and inner regions, proximity to the river mouths subject inshore mussels to large autumn/ winter river discharges that can propel large wave action and fluctuating salinity conditions though abundant food concentrations seemingly enables mussels to cope enough to compensate.

The spatial variability of the mussel epibiont *A. sphyrodeta* coincided with an interannual increase in upwelling index though further studies are required to determine a correlation, if any, and the role of abiotic and biotic factors in structuring their abundance and distribution. *A. sphyrodeta* plays a crucial role in mediating mussel attachment strength responses, and its blooms exert an environmental pressure that perpetuate harmful economic impacts to suspended mussel cultivation in the Ría de Arousa.

ACKNOWLEDGEMENTS

I thank E. Silva (IIM-CSIC) for technical assistance with collection and treatment of the mussels, X.A. Padín (IIM-CSIC) for providing the ROMS and chlorophyll a data, A. Martínez Fernández (IIM-CSIC) for collecting the wave parameter database, and my supervisors, M. Gil Coto and J.M. Fernandez Babarro for their diligent support and encouragement. This research was supported by the MYTIGAL project (AGL2013-45945-R) and co-funded by the European Regional Development Fund 2014-2020 (FEDER) and the ARIOS project (CTM2016-76146-C3-2-R), both also supported by the Spanish Ministry for Economy and Competitiveness. This work was supported by a CSIC JAE ICUs fellowship.

REFERENCES

Akester R.J., Martel A.L. (2000). Shell shape, dysodont tooth morphology and hinge-ligament thickness in the bay mussel *Mytilus trossulus* correlate with wave exposure. Can. J. Zool., 78: 240-253, https://doi.org/10.1139/Z99-215

Álvarez-Salgado X. A., Rosón G., Pérez F. F., Figueiras F. G., Ríos A.F. (1996). Nitrogen cycling in an estuarine upwelling system, the Ría de Arousa (NW Spain). II. Spatial differences in the short-time-scale evolution of fluxes and net budgets. Marine Ecology Progress Series, 135: 275-288, doi:10.3354/meps135275.

Álvarez-Salgado X. A., Gago J., Míguez B. M., Gilcoto M., Pérez F. F. (2000). Surface waters of the NW Iberian margin: upwelling on the shelf versus outwelling of upwelled waters from the Rías Baixas. Estuarine, Coastal and Shelf Science, 51(6): 821-837, doi:10.1006/ecss.2000.0714.

Arístegui J., Barton E. D., Álvarez-Salgado X. A., Santos A. M. P., Figueiras F. G., Kifani S., Hernández-León S., Mason E., Machú E., Demarcq H. (2009). Sub-regional ecosystem variability in the Canary Current upwelling. *Progress in Oceanography*, 83(1-4): 33-48, doi:10.1016/j.pocean.2009.07.031.

Babarro J.M.F., Abad M.J. (2013). Co-existence of two mytilid species in a heterogeneous environment: mortality, growth and strength of shell and byssus attachment. Mar Ecol Prog Ser 476:115-128, doi.org/10.3354/meps10122

Babarro J.M.F., Carrington E. (2011). Byssus secretion of Mytilus galloprovincialis: effect of site at macro- and micro-geographical scales within Ría de Vigo (NW Spain). Mar. Ecol. Prog. Ser. 435: 125–140, doi: 10.3354/ meps09200

Babarro J.M.F., Carrington E. (2013). Attachment strength of the mussel Mytilus galloprovincialis: effect of habitat and body size. J. Exp. Mar. Biol. Ecol. 443: 188–196, doi: 10.1016/j.jembe.2013.02.035

Babarro J.M.F., Comeau L.A. (2014). Byssus attachment strength of two mytilids in mono-specific and mixed-species mussel beds. Biofouling. 30: 975–985, doi:10.1080/ 08927014.2014.953941

Babarro J.M.F., Fernández-Reiriz M.J. (2010). Secretion of byssal threads in *Mytilus galloprovincialis* after spawning stress. J. Comp. Physiol. B 180: 95–104, https://doi.org/10.1007%2Fs00360-009-0392-y

Babarro J.M.F., Filgueira R., Padín X.A., Longa Portabales M.A. (2020). A Novel Index of the Performance of Mytilus galloprovincialis to Improve Commercial Exploitation in Aquaculture. Front. Mar. Sci. 7: 719, doi: 10.3389/fmars.2020.00719

Babarro J.M.F., Lassudrie M. (2011). Ecophysiological responses of invasive and indigenous mytilids in the Ría de Vigo (NW Spain). Aquat. Living Resour., 24 (03): 303-315, doi:10.1051/alr/2011142

Babarro J. M. F., Padín X. A., Filgueira R., Morabet H. E., Longa Portabales M. A. (2019). The

impact of the sea anemone Actinothoe sphyrodeta on Mytilus galloprovincialis mussel cultivation (Galicia, Spain). Biofouling 34: 1138–1149, doi: 10.1080/08927014.2018.1547818

Bakun A., (1973). Coastal upwelling indices, west coast of North America, 1946-71. U.S.Dep. Commer., NOAA Tech. Rep., NMFS SSRF-671, p 103

Barnston A. G., Livezey R. E. (1987). Classification, seasonality and persistence of low-frequency atmospheric circulation patterns. *Mon. Wea. Rev.*, 115: 1083-1126.

Beadman H.A., Caldow R.W.G., Kaiser M.J., Willows R.I. (2003). How to toughen up your mussels: using shell morphological plasticity to reduce predation losses. Mar. Biol., 142: 487-494, https://doi.org/10.1007/s00227-002-0977-4

Bell E.C., Gosline J.M. (1996). Mechanical design of mussel byssus: material yield enhances attachment strength. J Exp Biol 199: 1005-1017, https://doi.org/10.1242/jeb.199.4.1005

Bell E. C., Gosline J. M. (1997). Strategies for life in flow: tenacity, morphometry, and probability of dislodgement of two Mytilus species. Mar. Ecol. Prog. Ser. 159: 197–208. doi: 10.3354/meps159197

Blanton J. O., Atkinson L. P., Fernández de Castillejo F., Lavín Montero A. (1984). Coastal upwelling off the Rias Bajas, Galicia, Northwest Spain I: Hydrographic studies. Rapp. P-v. Reun. Cons. Int. Explor. Mer., 183: 79-90.

Blanton J. O., Tenore K. R., Castillejo F., Atkinson L. P., Schwing F. B., Lavín A. (1987). The relationship of upwelling to mussel production in the rias on the western coast of Spain. Journal of Marine Research, 45(2): 497-511, doi:10.1357/002224087788401115.

Carrington E. (2002). Seasonal variation in the attachment strength of blue mussels: causes and consequences. Limnol. Oceanogr. 47: 1723–1733. doi: 10. 4319/lo.2002.47.6.1723

Carrington E., Moeser G.M., Dimond J, Mello J.J., Boller M.L. (2009). Seasonal disturbance to mussel beds: Field test of a mechanistic model predicting wave dislodgment. *Limnology and Oceanography*, 54, doi: 10.4319/lo.2009.54.3.0978.

Carrington E., Waite J.H., Sará G., Sebens K.P. (2015). Mussels as a model system for integrative ecomechanics. Annu. Rev. Mar. Sci. 7: 443–469. doi: 10.1146/annurev-marine-010213-135049

Castelle B., Dodet G., Masselink G., Scott T. (2017). A new climate index controlling winter wave activity along the Atlantic coast of Europe: The West Europe Pressure Anomaly. Geophysical Research Letters, 44(3): 1384–1392. https://doi.org/10.1002/2016GL072379

Conover W. J. (2012). The rank transformation—an easy and intuitive way to connect many nonparametric methods to their parametric counterparts for seamless teaching introductory statistics courses. WIREs Comp. Stat. 4: 432– 438. doi: 10.1002/wics.1216

Debreu L., Marchesiello P., Penven P., Cambon G. (2012). Two-way nesting in split-explicit ocean models: algorithms, implementation and validation. Ocean Model., 49: 1-21,

https://doi.org/10.1016/j.ocemod.2012.03.003

Denny M.W. (1987). Lift as a mechanism of patch initiation in mussel beds. J. Exp. Mar. Biol. Ecol. 113: 231–245.

Denny M.W., Gaylord, B. (2010). Marine ecomechanics. Annual Review of Marine Science, 2(1): 89– 114. https://doi.org/10.1146/annurev-marine-120308-081011

Egbert G. D., Erofeeva S. Y. (2002). Efficient inverse modeling of barotropic ocean tides. *Journal of Atmospheric and Oceanic Technology*, 19(2): 183-204, doi:10.1175/1520-0426(2002)019<0183:EIMOBO>2.0.CO;2.

FAO (2022). The State of World Fisheries and Aquaculture 2022. Towards Blue Transformation. Rome, FAO. https://www.fao.org/3/cc0461en/cc0461en.pdf Accessed on 28 May 2023.

FAO (2023). The European market for mussels. https://www.fao.org/in-action/globefish/fishery-information/resource-detail/en/c/338588/ Accessed on 28 May 2023.

Figueiras F.G., Labarta U., Reiriz M.J. (2002). Coastal upwelling, primary production and mussel growth in the Rías Baixas of Galica. Hydrobilogia, 484, 121-131, doi:10.1023/A:1021309222459.

Floriolli RY, von Langen J, Waite JH. (2000). Marine Surfaces and the Expression of Specific Byssal Adhesive Protein Variants in Mytilus. Mar Biotechnol (NY). 2(4): 352-363. doi: 10.1007/s101269900032.

Fraga F. (1981). Upwelling off the Galician coast, northwest Spain, in *Coastal Upwelling*, Coastal and Esturarine Sci., vol. 1, Richards F.A. (Ed.), pp. 176–182, AGU, Washington, D.C.

Freeman K.R. (1974). Growth, Mortality and Seasonal Cycle of Mytilus edulis in Two Nova Scotian Embayments. Department of the Environment, Fisheries and Marine Service, Canada, Technical Report No. 500. Dartmouth, NS: Marine Ecology Laboratory, 112.

Freeman A.S., Meszaros J., Byers J.E. (2009). Poor phenotypic integration of blue mussel inducible defenses in environments with multiple predators. Oikos, 118: 758-766. https://doi.org/10.1111/j.1600-0706.2008.17176.x

Fuentes-Santos I., Labarta U., Álvarez Salgado X.A. (2019). Modelling mussel shell and flesh growth using a dynamic net production approach. Aquaculture 506: 84–93. https://doi.org/10.1016/j.aquaculture.2019.03.030.

Gardner J.P.A., Thomas M.L.H. (1987). Growth, mortality and production of organic matter by a rocky intertidal population of Mytilus edulis in the Quoddy Region of the Bay of Fundy. *Marine Ecology Progress Series*, *39*(1): 31–36. http://www.jstor.org/stable/24825643

Garner Y.L., Litvaitis M.K. (2013). Effects of wave exposure, temperature and epibiont fouling on byssal thread production and growth in the blue mussel, *Mytilus edulis*, in the Gulf of Maine. J. Exp. Mar. Biol. Ecol., 446: 52-56, doi.org/10.1016/j.jembe.2013.05.001

Green D.S., Colgan T.J., Thompson R.C., Carolan J.C. (2019). Exposure to microplastics reduces attachment strength and alters the haemolymph proteome of blue mussels (Mytilus edulis). Environ. Pollut., 246: 423-434, doi.org/10.1016/J.ENVPOL.2018.12.017

Griffiths C. L., King J.A. (1979). Energy expended on growth and gonad output in the ribbed mussel Aulacomya ater. Mar. Biol. 53: 217–222. doi: 10. 1007/BF00952429

Hawkins A.J.S., Bayne B.L. (1985). Seasonal variation in the relative utilization of carbon and nitrogen by the mussel Mytilus edulis: budgets, conversion efficiencies and maintenance requirements. Mar. Ecol. Progr. Ser. 25: 181–188. doi: 10.3354/meps025181

Instituto Español de Oceanografía (2011). Índice de Afloramiento. http://www.indicedeafloramiento.ieo.es/index_UI_es.html. Accessed 27 May 2009.

IPCC, 2022: Climate Change 2022: Impacts, Adaptation and Vulnerability. Contribution of Working Group II to the Sixth Assessment Report of the Intergovernmental Panel on Climate Change [H.-O. Pörtner, D.C. Roberts, M. Tignor, E.S. Poloczanska, K. Mintenbeck, A. Alegría, M. Craig, S. Langsdorf, S. Löschke, V. Möller, A. Okem, B. Rama (eds.)]. Cambridge University Press. Cambridge University Press, Cambridge, UK and New York, NY, USA, 3056 pp., doi:10.1017/9781009325844.

Lachance A. A., Myrand B., Tremblay R, Koutitonsky V, Carrington E. (2008). Biotic and abiotic factors influencing attachment strength of blue mussels Mytilus edulis in suspended culture. Aquatic Biology, 2: 119–129. https://doi.org/10.3354/ab00041

Largier J.L. (2020). Upwelling Bays: How Coastal Upwelling Controls Circulation, Habitat, and Productivity in Bays. *Annual Review of Marine Science*, 12: 415-447, doi:10.1146/annurev-marine-010419-011020.

Lavín A., Diaz del Rio G., Cabanas J.M., Casas G. (1991). Afloramiento en el Noroeste de la Peninsula Iberica. Indices de afloramiento para el punto 43º N 11º W. Periodo 1966-1989. Informes Técnicos del Instituto Español de Oceanografía, 91: 1-40. http://www.indicedeafloramiento.ieo.es/Documentos/informes_tecnico_ieo_91.pdf

Lesser M.P., Shumway S.E., Cucci T., Smith J. (1992). Impact of fouling organisms on mussel rope culture: interspecific competition for food among suspension-feeding invertebrates. J Exp Mar Biol Ecol, 165: 91–102. doi:10.1016/0022-0981(92)90291-H

Lucas J.M., Vaccaro E., Waite J.H. (2002). A molecular, morphometric and mechanical comparison of the structural elements of byssus from Mytilus edulis and Mytilus galloprovincialis. *The Journal of experimental biology*, *205*(12): 1807–1817. https://doi.org/10.1242/jeb.205.12.1807

Martinez M., Mangano C., Maricchiolo G., Genovese L., Mazzola A., Sarà G. (2018). Measuring the effects of temperature rise on Mediterranean shellfish aquaculture. Ecol. Indic. 88: 71–78. doi.org/10.1016/j.ecolind.2018.01.002

McDowell L.M., Burzio L.A., Waite J.H., Schaefer J. (1999). Rotational echo double resonance detection of cross-links formed in mussel byssus under high-flow stress. J. Biol.

Chem., 274: 20293-20295, doi.org/10.1074/jbc.274.29.20293

Mexillón de Galicia (2023a) Tradición histórica. Xunta de Galicia. https://www.mexillondegalicia.org/?page_id=20 Accessed on 29 May 2023.

Mexillón de Galicia (2023b) Las rías. Xunta de Galicia. https://www.mexillondegalicia.org/?page_id=22 Accessed on 29 May 2023.

MolluscaBase eds. (2023). MolluscaBase. *Mytilus galloprovincialis* Lamarck, 1819. Accessed through: World Register of Marine Species at: https://www.marinespecies.org/aphia.php?p=taxdetails&id=140481 Accessed on 12 May 2023.

Otto L. (1975). Oceanography of the Ría de Arosa (N.W. Spain). Koninklijk Nederlands Meteorologisch Instituut, Staatsuitgeverij/'S-Gravenhage, 211 pp.

Pardo P.C., Padín X.A., Gilcoto M., Farina-Busto L., Pérez F. F. (2011). Evolution of upwelling systems coupled to the long-term variability in the sea surface temperature and Ekman transport. *Climate Research*, 48(2-3): 231-246, doi:10.3354/cr00989.

Pérez F. F., Padín X.A., Pazos Y., Gilcoto M., Doval M.D., Cabanas J.M., Fariña-Busto L. (2010). Plankton response to weakening of coastal upwelling. *Global Change Biology*, 16(4): 1258-1267, doi:10.1111/j.1365-2486.2009.02125.x

Qin Z., Buehler M.J. (2013). Impact tolerance in mussel thread networks by heterogeneous material distribution. Nat Commun, 4: 2187, doi: 10.1038/ncomms3187.

Raubenheimer D., Cook P. (1990). Effects of exposure to wave action on allocation of resources to shell and meat growth by the subtidal mussel, Mytilus galloprovincialis. J Shellfish Res, 9: 87-93

Rosón G., Pérez F. F., Álvarez-Salgado X.A., Figueiras F.G. (1995). Variation of both thermohaline and chemical properties in an estuarine upwelling ecosystem : Ría de Arousa. I. Time evolution. Estuarine, Coastal and Shelf Science, 41(2): 195-213, doi:10.1006/ecss.1995.0061.

Rosón G., Álvarez-Salgado X.A., Pérez F. F. (1997). A non-stationary box model to determine residual fluxes in a partially mixed estuary, based on both thermohaline properties: Application to the Ria de Arousa (NW Spain). Estuarine, Coastal and Shelf Science, 44(3): 249-262, https://doi.org/10.1006/ecss.1996.0127

Rosón G., Álvarez-Salgado X.A., Pérez F. F. (1999). Carbon cycling in a large coastal embayment, affected by wind-driven upwelling: short-time-scale variability and spatial differences. Marine Ecology Progress Series, 176: 215-230, doi:10.3354/meps176215.

Scott T., Masselink G., Castelle B., Dodet G. (2020). *The West Europe Pressure Anomaly*, Dataset. University of Plymouth Pedagogic Research and Development Database, http://hdl.handle.net/10026.1/15509

Sievers M., Fitridge I., Dempster T., Keough M.J. (2013). Biofouling leads to reduced shell growth and flesh weight in the cultured mussel Mytilus galloprovincialis. Biofouling, 29 (1): 97-107, DOI: 10.1080/08927014.2012.749869

Steffani C.N., Branch G.M. (2003). Growth rate, condition, and shell shape of Mytilus galloprovincialis: responses to wave exposure. Mar. Ecol. Prog. Ser. 246: 197–209, doi: 10.3354/meps246197

Suchanek T.H. (1992). Extreme biodiversity in the marine environment: Mussel bed communities of Mytilus californianus. Northwest Environ. J., 8: 150–152.

The SWAN Team (2022). *SWAN User Manual*, Cycle III, version 41.41. Delft University of Technology, 154 pp, https://swanmodel.sourceforge.io/download/download.htm.

Vilas Martín F., Rey García D., Rubio Armesto B., Bernabeu Tello A., Méndez Martínez G., Duran Gallego R., Mohamed Falcón K. (2008). Los Fondos de la Ría de Vigo. In: González-Garcés Santiso A., Vilas Martín F., Álvarez Salgado X.A. (Eds). La Ría de Vigo, Instituto de Estudios Vigueses, pp. 17-50

Villacieros-Robineau N., Gilcoto M., Pardo P.C., Barton E.D. (2021). Wave Regime and Wave-Current Coupling in an Upwelling–Driven Bay: Seasonal and Inter-Annual Variability. *Journal of Geophysical Research: Oceans*, 126 (11), doi:10.1029/2021jc017540.

Waite J.H. (1992). The formation of mussel byssus: anatomy of a natural manufacturing process. In: Case S.T. (Ed.). Results and Problems in Cell Differentiation, Berlin: Springer-Verlag, 19: 27–54.

Watanabe S., Katayama S. (2010). Relationships among shell shape, shell growth rate, and nutritional condition in the Manila clam (Ruditapes philippinarum) in Japan. J. Shellfish Res. 29: 353–359, doi: 10.2983/035.029. 0210

WW3DG (The WAVEWATCH III Development Group) (2019). *User manual and system documentation of WAVEWATCH III*, version 6.07. Tech. Note 333, NOAA/ NWS/ NCEP/ MMAB, College Park, MD, USA, 465 pp. and appendices

Zardi G.I., McQuaid C.D., Nicastro K.R. (2007). Balancing survival and reproduction: seasonality of wave action, attachment strength and reproductive output in indigenous Perna perna and invasive Mytilus galloprovincialis mussels. Mar. Ecol. Progr. Ser. 334: 155–163, doi: 10.3354/meps334155

APPENDIX

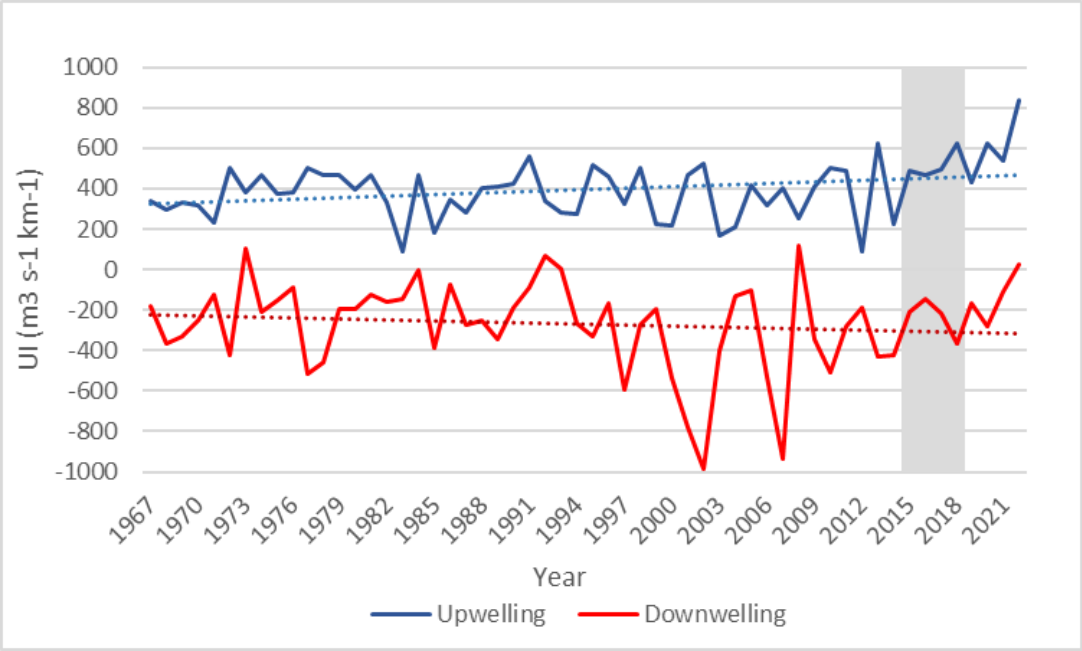

Figure 26. Annual variability of mean upwelling index (UI) for upwelling (blue) and downwelling (red) seasons from 1967 to 2022, study period shaded in gray.